BJ www.biochemj.org

Biochem. J. (2012) 441, 697–705 (Printed in Great Britain) doi:10.1042/BJ20111472

Chondroitin 4-*O*-sulfotransferase-2 regulates the number of chondroitin sulfate chains initiated by chondroitin *N*-acetylgalactosaminyltransferase-1

Tomomi IZUMIKAWA, Toshiyasu KOIKE and Hiroshi KITAGAWA[1]

Department of Biochemistry, Kobe Pharmaceutical University, Higashinada-ku, Kobe 658-8558, Japan

Recently, it has been shown that a deficiency in ChGn-1 (chondroitin *N*-acetylgalactosaminyltransferase-1) reduced the numbers of CS (chondroitin sulfate) chains, leading to skeletal dysplasias in mice. Although these results indicate that ChGn-1 regulates the number of CS chains, the mechanism mediating this regulation is not clear. ChGn-1 is thought to initiate CS biosynthesis by transferring the first GalNAc (*N*-acetylgalactosamine) to the tetrasaccharide in the protein linkage region of CS. However, *in vitro* chondroitin polymerization does not occur on the non-reducing terminal GalNAc-linkage pentasaccharide structure. In the present study we show that several different heteromeric enzyme complexes composed of different combinations of four chondroitin synthase family members synthesized more CS chains when a GalNAc-linkage pentasaccharide structure with a non-reducing terminal 4-O-sulfation was the CS acceptor. In addition, C4ST-2 (chondroitin 4-*O*-sulfotransferase-2) efficiently transferred sulfate from 3′-phosphoadenosine 5′-phosphosulfate to position 4 of non-reducing terminal GalNAc-linkage residues, and the number of CS chains was regulated by the expression levels of C4ST-2 and of ChGn-1. Taken together, the results of the present study indicate that C4ST-2 plays a key role in regulating levels of CS synthesized via ChGn-1.

Key words: chondroitin sulfate, glycosaminoglycan, glycosyltransferase, proteoglycan, sulfotransferase.

INTRODUCTION

CSs (chondroitin sulfates) are covalently bound to specific serine residues in the core regions of many proteins through a common carbohydrate–protein linkage tetrasaccharide GlcAβ1-3Galβ1-3Galβ1-4Xylβ1-*O*-Ser. Following the complete synthesis of the linkage-region tetrasaccharide, the first GalNAc (*N*-acetylgalactosamine) residue is transferred to a GlcA (glucuronic acid) residue in the linkage-region tetrasaccharide, triggering the synthesis of CS. Next, GlcA and GalNAc residues are alternately transferred on to growing CS chains, resulting in the formation of the polymer sugar backbone of CS [1]. After the synthesis of the CS sugar backbone on this tetrasaccharide, numerous modifications, including sulfation, occur under tight spatio-temporal regulation producing mature and functional GAG (glycosaminoglycan) chains that exert specific biological functions that are dependent on their specific structures.

To date, six glycosyltransferases involved in the biosynthesis of CS have been cloned. We and others have identified the six chondroitin-synthesizing enzymes: ChSy (chondroitin synthase)-1, ChSy-2, ChSy-3, ChPF (chondroitin-polymerizing factor) and ChGn (chondroitin GalNAc transferase)-1 and -2 [2–9]. ChSy-1, ChSy-2 and ChSy-3 show dual glycosyltransferase activities, GlcAT-II (GlcA transferase II) and GalNAcT-II (GalNAc transferase II), that are responsible for synthesizing the repeating disaccharide units of CS [2–4], and ChGn-1 and -2 catalyse chain initiation and elongation, exhibiting activities of GalNAcT-I and -II [6–9]. In addition, seven sulfotransferases involved in the sulfation of CS, including four sulfotransferases involved in the sulfation of position 4 of the GalNAc residue, have been cloned [10]. C4STs (chondroitin 4-*O*-sulfotransferases)-1, -2 and -3 are responsible for the sulfation of position 4 of the GalNAc residues in CS, whereas D4ST-1 (dermatan 4-*O*-sulfotransferase-1) catalyses the transfer of sulfate residues to GalNAc residues located next to IdoUA (iduronic acid) residues in DS (dermatan sulfate) [11–15]. C6ST-1 (chondroitin 6-*O*-sulfotransferase-1) transfers sulfate to position 6 of GalNAc residues [16,17]. The 2-O-sulfation of GlcA and IdoUA is catalysed by uronyl 2-*O*-sulfotransferase [18]. GalNAc4S-6ST (GalNAc 4-sulfate 6-*O*-sulfotransferase) transfers a sulfate residue to position 6 of GalNAc(4-*O*-sulfate) formed by C4ST [19].

Previously, we demonstrated that chondroitin is polymerized with alternating GalNAc and GlcA residues on the linkage-region tetrasaccharide of α-TM (α-thrombomodulin) when any two of four proteins, ChSy-1, ChSy-2, ChSy-3 and ChPF, were co-expressed [3–5]. These results indicated that ChGn-1 and ChGn-2, both of which have both GalNAcT-I and -II activity, were dispensable for chondroitin polymerization on the linkage-region tetrasaccharide [3–5]; however, recently it was shown that a deficiency in ChGn-1 reduced the number of CS chains, leading to skeletal dysplasias in mice [20]. Taken together, these results indicate that the transfer of a single GalNAc residue to the tetrasaccharide linkage region by ChGn-1 and the activity of chondroitin polymerases comprising any two of the ChSy-1, ChSy-2, ChSy-3 and ChPF proteins are both important for efficient biosynthesis of CS chains.

Given these findings, we hypothesized that the non-reducing terminal GalNAc-linkage structure formed by ChGn-1 would markedly enhance the number of CS chains produced by chondroitin polymerases comprising any two of the ChSy-1, ChSy-2, ChSy-3 and ChPF proteins (Figure 1). However, the results of the present study demonstrated that a non-reducing terminal GalNAc-linkage structure did not serve as a chondroitin polymerization substrate. In the present paper we report that

Abbreviations used: ChGn, chondroitin *N*-acetylgalactosaminyltransferase; ChPF, chondroitin-polymerizing factor; ChSy, chondroitin synthase; CS, chondroitin sulfate; C4ST, chondroitin 4-*O*-sulfotransferase; D4ST-1, dermatan 4-*O*-sulfotransferase-1; GAG, glycosaminoglycan; GalNAc, *N*-acetylgalactosamine; GalNAcT, GalNAc transferase; GAPDH, glyceraldehyde-3-phosphate dehydrogenase; GlcA, glucuronic acid; IdoUA, iduronic acid; OA, osteoarthritis; PAPS, 3′-phosphoadenosine 5′-phosphosulfate; RT, reverse transcription; shRNA, short hairpin RNA; α-TM, α-thrombomodulin.

[1] To whom correspondence should be addressed (email kitagawa@kobepharma-u.ac.jp).

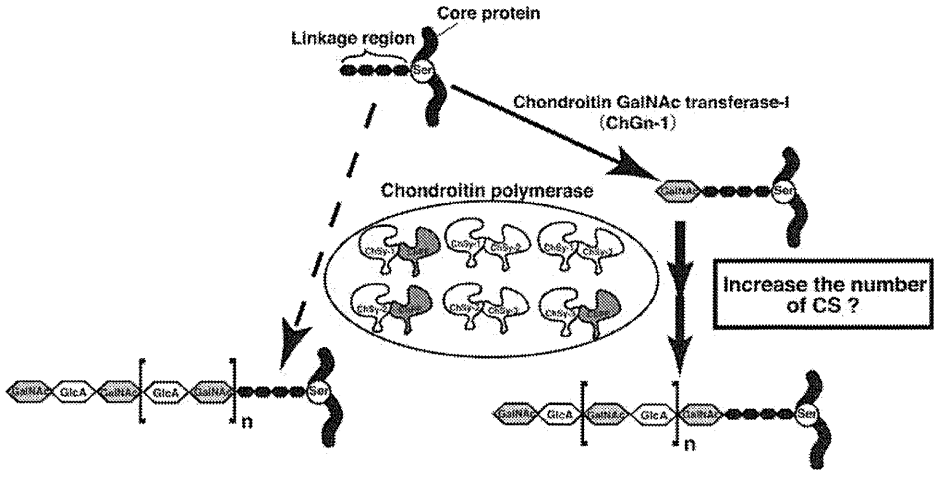

Figure 1 Initiation of CS polymerization

CS is synthesized as proteoglycans on specific serine residues in the GAG-protein linkage region, GlcAβ1-3Galβ1-3Galβ1-4Xylβ1-*O*-Ser. Following the complete synthesis of the linkage-tetrasaccharide sequence, the transfer of a single GalNAc residue to the tetrasaccharide linkage region by any two of ChSy-1, ChSy-2, ChSy-3 or ChPF (broken line), or by ChGn-1 (solid line) initiates the assembly of CS. Thus it was expected that the non-reducing terminal GalNAc-linkage structure formed by ChGn-1 would markedly enhance the number of CS chains produced by chondroitin polymerases, meaning any two of ChSy-1, ChSy-2, ChSy-3 and ChPF.

a non-reducing terminal GalNAc(4-*O*-sulfate)-linkage structure on CS resulted in an increase in the number of CS chains that were synthesized by multiple enzyme complexes comprising combinations of four ChSy family members and that C4ST-2 was involved in the mechanism that resulted in an increase in the number of CS chains that was mediated by ChGn-1.

EXPERIMENTAL

Materials

UDP-[^{3}H]GalNAc (10 Ci/mmol) was purchased from NEN Life Science Products, and ^{35}S-labelled PAPS (3′-phosphoadenosine 5′-phosphosulfate) (1.69 mCi/mmol) was purchased from PerkinElmer Life Sciences. Unlabelled UDP-GlcA, UDP-GalNAc and PAPS were obtained from Sigma. Chondroitinase ABC isolated from *Proteus vulgaris* (EC 4.2.2.20) and chondroitinase ACII isolated from *Arthrobacter aurescens* (EC 4.2.2.5) were purchased from Seikagaku. Superdex™ Peptide HR10/30 and Superdex™ 200 10/300 GL columns were purchased from Amersham Pharmacia Biotech. α-TM with a truncated linkage-region tetrasaccharide, GlcAβ1-3Galβ1-3Galβ1-4Xyl, was purified and structurally characterized as described previously [21,22].

Polymerization assay and identification of polymerization reaction products

First, a GalNAc transfer reaction was conducted; α-TM that contained the linkage-region tetrasaccharide GlcAβ1-3Galβ1-3Galβ1-4Xyl (1 nmol) was used as an acceptor in the incubation mixture, which contained the following constituents in a total volume of 20 μl: 10 μl of the soluble form of ChGn-1-bound beads [6] as the enzyme source, 0.25 mM UDP-GalNAc or UDP-[^{3}H]GalNAc (2×10^5 d.p.m.), 100 mM Mes buffer (pH 5.8) and 10 mM $MnCl_2$. Then, the reaction products were separated by gel-filtration chromatography on a Superdex™ peptide column that had been equilibrated and eluted with 0.25 M NH_4HCO_3/7 % propan-1-ol. Next, 4-O-sulfation of the GalNAc residue was performed using GalNAc-TM (GalNAcβ1-4GlcAβ1-3Galβ1-3Galβ1-4Xylβ1-*O*-TM) (1 nmol) as an acceptor in an incubation mixture, which contained the following constituents in a total volume of 30 μl: 10 μl of the soluble form of C4ST-2-bound beads [15] as the enzyme source, 50 mM imidazole/HCl (pH 6.8), 2 mM dithiothreitol and 10 μM [^{35}S]PAPS (3×10^5 d.p.m.). Then, the reaction products were separated by gel-filtration chromatography on a Superdex™ peptide column that had been equilibrated and eluted with 0.25 M NH_4HCO_3/7 % propan-1-ol. The fractions containing the enzyme reaction products were pooled and evaporated to dryness. The isolated reaction products were used as substrates for polymerization reactions. Polymerization reactions were simultaneously incubated in parallel in reaction mixtures containing the following constituents in a total volume of 20 μl: 1 nmol of [^{3}H]GalNAc-TM or [^{35}S]GalNAc(4-*O*-sulfate)β1-4GlcAβ1-3Galβ1-3Galβ1-4Xylβ1-*O*-TM {[^{35}S]GalNAc(4S)-TM}, 0.25 mM UDP-GalNAc, 0.25 mM UDP-GlcA, 100 mM Mes buffer (pH 6.5), 10 mM $MnCl_2$, and 10 μl of the soluble form of ChSy-1–ChPF-, ChSy-1–ChSy-2-, ChSy-1–ChSy-3-, ChSy-2–ChPF-, ChSy-2–ChSy-3- or ChSy-3–ChPF-bound beads. The mixtures were incubated at 37 °C overnight, and the ^{3}H- or ^{35}S-labelled products were then separated by gel-filtration chromatography on a Superdex™ 200 column equilibrated and eluted with 0.25 M NH_4HCO_3/7 % propan-1-ol. Fractions (0.4 ml each) were collected at a flow rate of 0.4 ml/min, and radioactivity was measured with a liquid scintillation counter.

Establishment of an expression vector for ChGn-1 and preparation of cells that stably expressed ChGn-1

A cDNA fragment encoding *ChGn-1* (HUGO nomenclature *CSGALNACT1*) was amplified by RT (reverse transcription) using total RNA from G361 human melanoma cells (A.T.C.C. CRL-1424) as a template, and the forward primer 5′-CGGGAT-CCTCTGGACGCATGGCTGATTC-3′ and the reverse primer 5′-CGGGATCCCAGCTGGCACTGCCCAGG-3′; each primer contained a BamHI site. PCR was performed with KOD-Plus DNA polymerase (TOYOBO) for 30 cycles at 94 °C for 30 s, 58 °C for 42 s and 68 °C for 180 s in 5 % (v/v) DMSO. The

PCR fragments were subcloned into the BamHI sites of the pCMV expression vector (Invitrogen). The insert of the plasmid constructs (pCMV-ChGn-1) was confirmed by DNA sequencing. The expression plasmid (6.7 μg) was transfected into L and sog9 cells on 100-mm plates using FuGENE® 6 (Roche Applied Science), according to the manufacturer's protocol. Transfectants were cultured in the presence of 300 μg/ml G418, after which the resistant colonies were picked and propagated for experiments.

ChGn-1 silencing in L cells was performed using MISSION shRNA (short hairpin RNA) (Sigma). Plasmids (6.7 μg) encoding shRNA were transfected into L cells on 100-mm plates using FuGENE® 6 according to the manufacturer's protocol. Transfectants were cultured in the presence of 0.4 mg/ml puromycin. Resistant colonies were then picked and propagated for experiments.

Quantitative real-time RT–PCR

Total RNA was extracted from L cells or sog9 cells using TRIzol® reagent (Invitrogen). The cDNA was synthesized from ~1 μg of total RNA using Moloney murine leukemia virus reverse transcriptase (Promega) and oligo(dT)$_{20}$-M4 adaptor primers (TaKaRa). The primer sequences used were as follows: ChGn-1, forward primer 5′-AGAAGAAATAAATGAAGTCAAAGGAATAC-3′ and reverse primer 5′-GAAGTAGTAGTCCACATCACAG-3′; ChGn-2, forward primer 5′-CCTAGAATCTGTCACCAGT-3′ and reverse primer 5′-GTTAAGGAATTCGGCTGAGAAATA-3′; C4ST-1, forward primer 5′-ACCTCGTGGGCAAGTATGAG-3′ and reverse primer 5′-TCTGGAAGAACTCCGTGGTC-3′; C4ST-2, forward primer 5′-ATCAGCATCACCAGCAACA-3′ and reverse primer 5′-TGTGGCCTGGAGAGAGAC-3′; and GAPDH (glyceraldehyde-3-phosphate dehydrogenase), forward primer 5′-CATCTGAGGGCCCACTG-3′ and reverse primer 5′-GAGGCCATGTAGGCCATGA-3′. Quantitative real-time RT–PCR was performed using a FastStart DNA Master plus SYBR Green I kit (Roche Diagnostics) in a LightCycler ST300 (Roche Diagnostics). The expression levels of *ChGn-1*, *ChGn-2*, *C4ST-1* (HUGO nomenclature *CHST11*) or *C4ST-2* (HUGO nomenclature *CHST12*) mRNA were normalized to that of the *GAPDH* transcript.

Derivatization of GAGs from L and sog9 cells using a fluorophore, 2-aminobenzamide

GAGs from L and sog9 cells were prepared as described previously [23]. The purified GAG fraction was digested with chondroitinase ABC, and the digests were then derivatized with 2-aminobenzamide and analysed by HPLC as described previously [24].

Gel-filtration chromatography of GAGs

To measure the GAG chain lengths, the purified GAG fraction was subjected to reductive β-elimination using $NaBH_4$/NaOH, and then analysed by gel-filtration chromatography on a Superdex™ 200 column (10 mm×300 mm) eluted with 0.2 M ammonium bicarbonate at a flow rate of 0.4 ml/min. Fractions were collected at 3-min intervals, freeze-dried and digested with chondroitinase ABC. The digests were derivatized with 2-aminobenzamide, and then analysed by HPLC on an amine-bound PA-03 column, as described previously [24,25].

Expression of the soluble forms of the recombinant C4ST-1, C4ST-2 and D4ST-1, and identification of the reaction products

Each expression plasmid (6.0 μg) was transfected into COS-1 cells on 100-mm plates using FuGENE® 6 according to the manufacturer's protocol and as described previously [15]. At 2 days after transfection, 1 ml of the culture medium was collected and incubated with 10 μl of IgG–Sepharose (Amersham Pharmacia Biotech) for 1 h at 4 °C. The beads recovered by centrifugation (150 *g* at 4 °C for 5 min) were washed with and then resuspended in the assay buffer [50 mM imidazole/HCl (pH 6.8)], and the washed beads were tested for sulfotransferase activity. The assays used to detect sulfotransferase have been described previously [15] and were used with slight modifications. Briefly, the standard reaction mixture (30 μl) contained 10 μl of resuspended beads, 50 mM imidazole/HCl (pH 6.8), 2 mM dithiothreitol, 10 μM [^{35}S]PAPS (3×10^5 d.p.m.) and 1 nmol of GalNAc-TM as an acceptor substrate. The reaction mixtures were incubated at 37 °C overnight and subjected to gel filtration using the Superdex™ peptide column with 0.25 M NH_4HCO_3/7 % propan-1-ol as the eluent. The radioactive fractions containing the enzyme reaction products were pooled and evaporated to dryness. The isolated reaction products were subjected to reductive β-elimination using $NaBH_4$/NaOH, and then digested with chondroitinase AC-II. The enzymatically digested products were analysed using the Superdex™ peptide column with 0.25 M NH_4HCO_3/7 % propan-1-ol as the eluent.

Construction of an expression vector for C4ST-2 and preparation of cells that stably expressed C4ST-2

A cDNA fragment encoding *C4ST-2* was amplified using mouse heart Marathon-Ready cDNA (Clontech) as a template by two-round PCR using specific primer sets. The first PCR was performed with the forward primer 5′-CCAGCTGTGCACAAGGCTGA-3′ and the reverse primer 5′-TGCCTGTCACACCAGGAAGC-3′, followed by nested PCR with the nested forward primer 5′-GCACAAGGCTGAAGTGAAGG-3′ and the reverse primer 5′-AAGGAAGCCAGGAGAGAACC-3′. Each PCR was carried out using KOD-Plus in the presence of 5 % (v/v) DMSO and was subjected to 30 cycles at 94 °C for 30 s, 55 °C for 42 s, and 68 °C for 2.5 min. Amplified cDNA fragments of the expected size (~1.4 kb) were purified and subcloned into pGEM®-T Easy vectors (Promega). The cDNA encoding a full-length form of C4ST-2 from pGEM®-T Easy-C4ST-2 vectors was digested with EcoRI and subcloned into the EcoRI site of a pCMV expression vector. The insert of the plasmid constructs (pCMV-C4ST-2) was confirmed by DNA sequencing. The expression plasmid (6.7 μg) was transfected into L or sog9 cells on 100-mm plates using FuGENE® 6, according to the manufacturer's protocol. Transfectants were cultured in the presence of 300 μg/ml G418, after which the resistant colonies were picked and propagated for experiments.

RESULTS

A GalNAc-linkage structure did not serve as a chondroitin polymerization substrate

Recently, it has been shown that *ChGn-1*-deficient mice showed a 50 % decrease in CS levels in developing cartilage and a delay in cartilage development [20]. These results indicated that the non-reducing terminal GalNAc-linkage structure formed by ChGn-1 could markedly enhance the production of CS chains mediated by chondroitin polymerases that synthesize the CS backbone. Previously, we demonstrated that chondroitin

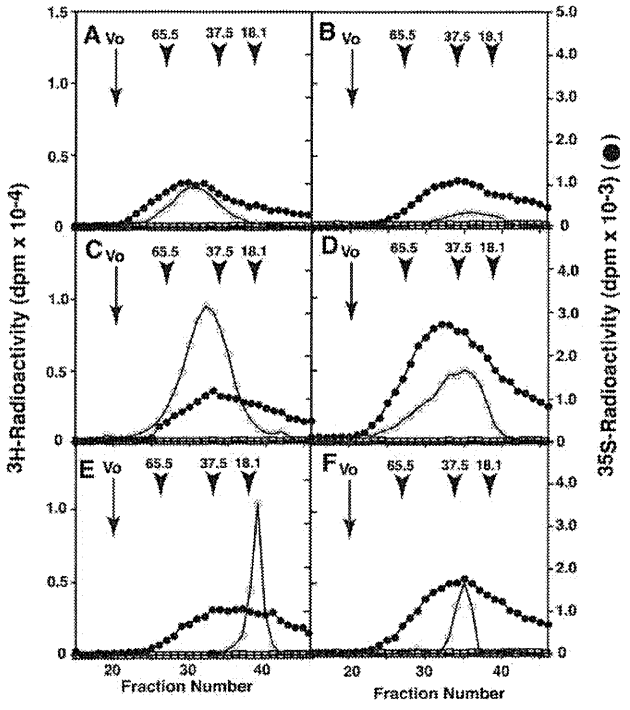

Figure 2 Comparison of CS chain lengths polymerized using various acceptors containing different non-reducing terminal structures

α-TM (○), which is a part-time proteoglycan and bears a truncated linkage region tetrasaccharide (GlcAβ1-3Galβ1-3Galβ1-4Xyl), [^{3}H]GalNAc-TM (□), which bears the non-reducing terminal GalNAc-linkage pentasaccharide, and the ^{35}S-labelled pentasaccharide TM [^{35}S]GalNAc(4S)-TM (●), were each tested as acceptors of polymerization reactions, and the co-expressed ChSy-1 and ChPF (**A**), ChSy-1 and ChSy-2 (**B**), ChSy-1 and ChSy-3 (**C**), ChSy-2 and ChPF (**D**), ChSy-2 and ChSy-3 (**E**), and ChSy-3 and ChPF (**F**) were used as the enzyme source, as described in the Experimental section. ^{3}H-Labelled or ^{35}S-labelled polymerization reaction products were first isolated by gel filtration, subjected to reductive β-elimination using $NaBH_4$/NaOH, and then rechromatographed on a Superdex™ 200 column with 0.25 M NH_4HCO_3/7 % propan-1-ol as the eluent. Arrowheads numbered 65.5, 37.5 and 18.1 indicate the eluted position of 65.5 kDa saccharides, 37.5 kDa saccharides and 18.1 kDa saccharides respectively, derived from commercial polysaccharides of known sizes (dextran average molecular masses of 200 kDa, 65.5 kDa, 37.5 kDa and 18.1 kDa; all from Sigma). The total volume was a fraction of ~60 (not shown).

polymerization takes place when any two of four proteins (ChSy-1, ChSy-2, ChSy-3 or ChPF) were co-expressed and the acceptor substrate was α-TM with a truncated linkage-region tetrasaccharide, GlcAβ1-3Galβ1-3Galβ1-4Xyl [3–5]. Therefore in the present study we measured polymerization activity using α-TM or [^{3}H]GalNAc-TM with the non-reducing terminal GalNAc-linkage pentasaccharide structure as an acceptor substrate and co-expression of any two of the ChSy-1, ChSy-2, ChSy-3 and ChPF proteins as the enzyme source (see the Experimental section). Polymerization did not occur with any enzyme subunit combination when [^{3}H]GalNAc-TM was the acceptor substrate (Figure 2, open squares). These results indicated that the non-reducing terminal GalNAc-linkage structure did not serve as a chondroitin polymerization substrate.

Involvement of ChGn-1 in increasing the number of CS chains

Previously, we found that overexpression of ChGn-1 slightly increases CS levels in L cells (see Table 2 in [26]). This result indicates that ChGn-1 might regulate the production of CS. Therefore we examined the effects of shRNA-mediated knockdown of ChGn-1 in L cells in the present study. The efficiency of gene shRNA-mediated silencing was determined by quantitative real-time RT–PCR. Transfection with ChGn-1 shRNA (L-shRNA ChGn-1-1 and L-shRNA ChGn-1-2 cells: two different shRNAs targeted against *ChGn-1* were used) resulted in a 60–80 % reduction in steady-state *ChGn-1* mRNA and an 18–22 % decrease in CS when compared with control L cells (Table 1). These findings indicate that the knockdown of ChGn-1 decreases CS levels in L cells, corresponding to expression levels of ChGn-1 (Table 1).

We next compared the CS chain lengths in L-shRNA ChGn-1-1, L-shRNA ChGn-1-2, and mock-transfected L cells. Gel-filtration analysis using a Superdex™ 200 column revealed that the length of CS chains in L-shRNA ChGn-1-1- and L-shRNA ChGn-1-2-transfected cells was similar to that in mock-transfected cells (Figure 3). Thus both *in vitro* and *in vivo* studies have shown that ChGn-1 regulates the number of CS chains, in spite of the fact that chondroitin polymerization did not occur on the non-reducing terminal GalNAc-linkage structure.

Involvement of the GalNAc(4-*O*-sulfate)-linkage structure in chondroitin polymerization

We recently found that the non-reducing terminal 4-O-sulfation of GalNAc residues on the repeating disaccharide region synthesized by C4ST-1 and ChGn-2 facilitates the elongation of CS chains only by chondroitin polymerase consisting of ChSy-1 and ChPF [26]. On the basis of this result, we predicted that the non-reducing terminal 4-O-sulfation of newly synthesized GalNAc-linkage regions might promote the elongation of CS chains by chondroitin polymerases. We measured polymerization activity using [^{35}S]GalNAc(4S)-TM as acceptor substrates, and the co-expression of any combination of two ChSy-1, ChSy-2, ChSy-3 and ChPF as the enzyme source. Reaction products obtained were subjected to reductive β-elimination using $NaBH_4$/NaOH, and the radiolabelled saccharides released were analysed by gel-filtration chromatography using a Superdex™ 200 column. Chondroitin polymerization was induced on the [^{35}S]GalNAc(4S)-TM when any combination of protein subunits was used as the enzyme source (Figure 2, closed circles). Notably, the length of the chondroitin chains synthesized on [^{35}S]GalNAc(4S)-TM by ChSy-1–ChPF, ChSy-1–ChSy-3 or ChSy-3–ChPF, and on α-TM were comparable (Figures 2A, 2C and 2F), but the chondroitin chains polymerized on [^{35}S]GalNAc(4S)-TM by ChSy-1–ChSy-2, ChSy-2–ChPF or ChSy-2–ChSy-3 were longer than those formed on α-TM (Figures 2B, 2D and 2E). These results indicated that chondroitin polymerization was facilitated by the non-reducing terminal GalNAc(4-*O*-sulfate)-linkage structure. Thus multiple enzyme complexes, which each comprised any two of four ChSy family members, synthesized more CS chains when there was a non-reducing terminal GalNAc(4-*O*-sulfate)-linkage structure on the CS acceptor substrate.

Identification of sulfotransferases involved in the 4-O-sulfation of the GalNAc-linkage pentasaccharide

Reportedly, C4ST-1, C4ST-2 and D4ST-1 catalyse the transfer of sulfate from PAPS to position 4 of the internal GalNAc residue of chondroitin [14,15]. However, it is not clear whether C4ST-1, C4ST-2 or D4ST-1 is also responsible for transferring the sulfate to position 4 of the non-reducing terminal GalNAc-linkage residue. Hence, we examined whether C4ST-1, C4ST-2 and/or D4ST-1 could sulfate the GalNAc-linkage residue. For this analysis, the recombinant C4ST-1, C4ST-2 and D4ST-1 were expressed and initially evaluated for sulfotransferase activities towards internal GalNAc residues using polymer

Table 1 Disaccharide composition of CS in mock- and shChGn-1-transfected L cells

Values are expressed as pmol of disaccharide per mg of dried homogenate of the cells and are means ± S.E.M. for three determinations. ΔDi-0S, ΔHexA(α1-3)GalNAc; ΔDi-6S, ΔHexAα1-3GalNAc(6-*O*-sulfate); ΔDi-4S, ΔHexAα1-3GalNAc(4-*O*-sulfate); ΔDi-diS$_D$, ΔHexA(2-*O*-sulfate)α1-3GalNAc(6-*O*-sulfate); ΔDi-diS$_E$, ΔHexAα1-3GalNAc(4-*O*-sulfate,6-*O*-sulfate); N.D., not detected (<0.01 pmol/mg).

(a) Composition

Disaccharide	L-mock [pmol/mg (mol%)]	L-shRNA ChGn-1-1 [pmol/mg (mol%)]	L-shRNA ChGn-1-2 [pmol/mg (mol%)]
ΔDi-0S	34 ± 8 (5)	20 ± 1 (7)	14 ± 1 (6)
ΔDi-6S	4 ± 2 (1)	13 ± 1 (5)	11 ± 1 (4)
ΔDi-4S	251 ± 18 (76)	210 ± 16 (78)	199 ± 19 (77)
ΔDi-diS$_D$	N.D.	N.D.	N.D.
ΔDi-diS$_E$	39 ± 9 (12)	27 ± 4 (10)	34 ± 3 (13)
Total (pmol/mg)	328 ± 20	270 ± 22	258 ± 25

(b) Relative expression

Transcript	L-mock	L-shRNA ChGn-1-1	L-shRNA ChGn-1-2
Relative expression of *ChGn-1**	1.0	0.4	0.2
Relative expression of *ChGn-2*	1.0	1.0	1.2
Relative expression of *C4ST-1*	1.0	0.9	1.1
Relative expression of *C4ST-2*	1.0	1.1	1.3

*Relative amounts of the *ChGn-1* transcript were quantified by quantitative real-time RT–PCR. *ChGn-1* mRNA expression values were normalized to *GAPDH* mRNA levels and are given relative to those in L cells.

Table 2 Disaccharide composition of CS in mock-, C4ST-2- and shC4ST-2-transfected L cells

Values are expressed as pmol of disaccharide per mg of dried homogenate of the cells and are means ± S.E.M. for three determinations. ΔDi-0S, ΔHexA(α1-3)GalNAc; ΔDi-6S, ΔHexAα1-3GalNAc(6-*O*-sulfate); ΔDi-4S, ΔHexAα1-3GalNAc(4-*O*-sulfate); ΔDi-diS$_D$, ΔHexA(2-*O*-sulfate)α1-3GalNAc(6-*O*-sulfate); ΔDi-diS$_E$, ΔHexAα1-3GalNAc(4-*O*-sulfate,6-*O*-sulfate); N.D., not detected (<0.01 pmol/mg).

(a) Composition

Disaccharide	L-mock [pmol/mg (mol%)]	L-C4ST-2-1 [pmol/mg (mol%)]	L-C4ST-2-2 [pmol/mg (mol%)]	L-shRNA C4ST-2-1 [pmol/mg (mol%)]	L-shRNA C4ST-2-2 [pmol/mg (mol%)]
ΔDi-0S	54 ± 6 (15)	110 ± 7 (16)	85 ± 4 (15)	47 ± 1 (20)	33 ± 4 (17)
ΔDi-6S	6 ± 2 (2)	11 ± 5 (2)	31 ± 3 (5)	7 ± 1 (3)	3 ± 1 (2)
ΔDi-4S	250 ± 20 (70)	472 ± 23 (69)	393 ± 7 (69)	150 ± 2 (63)	132 ± 19 (69)
ΔDi-diS$_D$	N.D.	N.D.	N.D.	N.D.	N.D.
ΔDi-diS$_E$	48 ± 12 (13)	89 ± 6 (13)	60 ± 4 (11)	35 ± 4 (15)	22 ± 3 (12)
Total (pmol/mg)	358 ± 8	682 ± 19	569 ± 12	239 ± 6	190 ± 25

(b) Relative expression

Transcript	L-mock	L-C4ST-2-1	L-C4ST-2-2	L-shRNA C4ST-2-1	L-shRNA C4ST-2-2
Relative expression of *C4ST-2**	1.0	7.6	3.4	0.3	0.2
Relative expression of *C4ST-1*	1.0	0.8	1.2	0.8	1.0
Relative expression of *ChGn-1*	1.0	0.9	0.9	1.1	1.0
Relative expression of *ChGn-2*	1.0	1.0	1.0	1.0	1.2

*Relative amounts of the *C4ST-2* transcript were quantified by quantitative real-time RT–PCR. *C4ST-2* mRNA expression values were normalized to *GAPDH* mRNA levels and are given relative to those in L cells.

chondroitin as an acceptor [15]. The activity of C4ST-1, C4ST-2 or D4ST-1 was 550, 81 or 89 pmol/μg per h respectively. Then, sulfotransferase activity was determined using GalNAc-TM as the acceptor substrate and [^{35}S]PAPS as the donor substrate. C4ST-2 transferred sulfate to GalNAc-TM much more efficiently than did C4ST-1 (Figure 4A). D4ST-1 showed no activity when GalNAc-TM was used as an acceptor (Figure 4A, open triangles, inset). To identify the ^{35}S-labelled products synthesized on the GalNAc-linkage pentasaccharide of α-TM, the products were subjected to reductive β-elimination and then digested to completion with chondroitinase AC-II, which cleaves the β1-4-*N*-acetylgalactosaminidic linkage. The digests were separated by gel-filtration chromatography using a Superdex™ peptide column, and a large peak was detected at the position corresponding to GalNAc-4-*O*-SO$_4$ (Figure 4B, closed circles). In sharp contrast, C4ST-1 transferred sulfate to the GalNAc residues and to a Gal residue of the linkage region, albeit transfer to the linkage region was much less efficient (Figure 4B, open circles, inset). These results indicated that C4ST-2 efficiently and selectively transferred sulfate from PAPS to the non-reducing terminal GalNAc-linkage residue.

Introduction of ChGn-1 to sog9 cells

Previously we found that C4ST-1 regulates the 4-O-sulfation of CS and the length and amount of CS chains [23], and that,

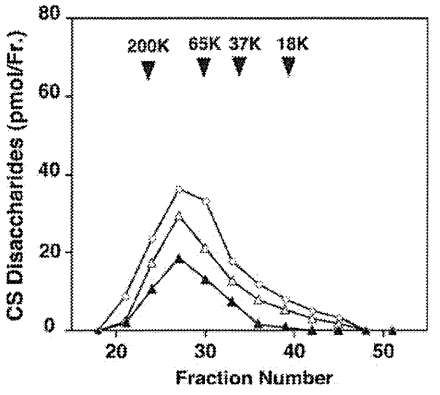

Figure 3 Analysis of the length of CS chains from L, L-shRNA ChGn-1-1 and L-shRNA ChGn-1-2 cells

Purified CS fractions were subjected to reductive β-elimination using $NaBH_4$/NaOH and then analysed by gel-filtration chromatography on a Superdex™ 200 column (10 mm×300 mm). The digests of individual fractions obtained with chondroitinase ABC were derivatized with 2-aminobenzamide and then analysed by HPLC. The amounts of the 2-aminobenzamide derivatives of unsaturated disaccharides were calculated based on fluorescence intensity. Samples from L-shRNA ChGn-1-1 (△), L-shRNA ChGn-1-2 (▲) and mock-transfected L (○) cells are shown. Arrowheads indicate the size of molecular mass standards in kDa. Data represent one of a series of three independent experiments, where all three experiments gave essentially the same results.

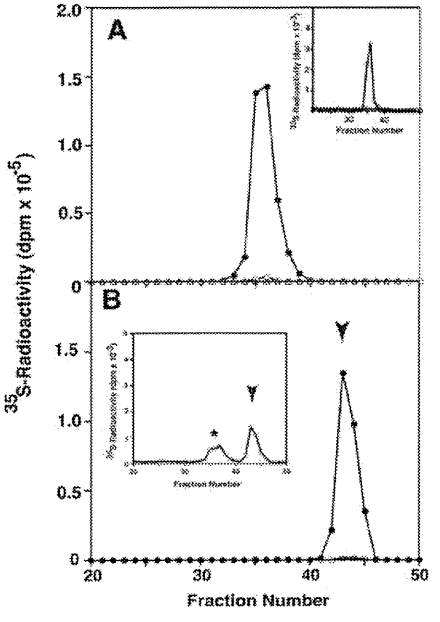

Figure 4 Identification of ^{35}S-labelled sulfotransferase reaction products prepared using C4ST-1, C4ST-2 and D4ST-1 as the enzyme sources

(**A**) GalNAcβ1-4GlcAβ1-3Galβ1-3Galβ1-4Xylβ1-*O*-TM was tested as a potential acceptor for sulfotransferase reactions, where C4ST-1 (○), C4ST-2 (●) or D4ST-1 (△) was used as an enzyme source, as described in the Experimental section. ^{35}S-Labelled sulfotransferase reaction products were first isolated by gel filtration, subjected to reductive β-elimination using $NaBH_4$/NaOH, and then rechromatographed on a Superdex™ peptide column with 0.25 M NH_4HCO_3/7 % propan-1-ol as the eluent. The inset shows a different scaling when C4ST-1 (○) or D4ST-1 (△) was used as an enzyme source. (**B**) ^{35}S-Labelled sulfotransferase reaction products were digested with chondroitinase AC-II. The chondroitinase AC-II digests derived from reaction products using C4ST-1 (○) or C4ST-2 (●) were isolated by gel filtration on a Superdex™ peptide column using 0.25 M NH_4HCO_3/7 % propan-1-ol as the eluent. The inset shows a different scaling when C4ST-1 (○) was used as an enzyme source. The arrowhead indicates the elution position of GalNAc-4-SO_4. The peaks marked by an asterisk indicate the elution position of GlcAβ-Gal(4-*O*-sulfate)-Gal-Xyl-ol.

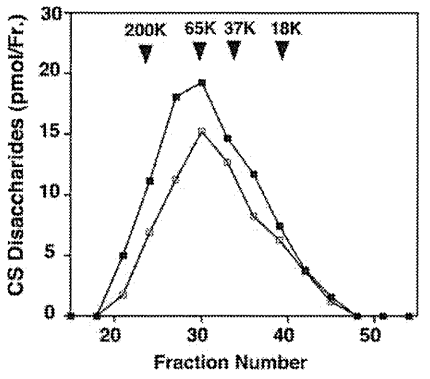

Figure 5 Analysis of the length of CS chains in sog9 and sog9-ChGn-1-1 cells

Purified CS fractions were subjected to reductive β-elimination using $NaBH_4$/NaOH and then analysed by gel-filtration chromatography on a Superdex™ 200 column (10 mm×300 mm). The digests of individual fractions obtained with chondroitinase ABC were derivatized with 2-aminobenzamide and then analysed by HPLC. The amounts of the 2-aminobenzamide derivatives of unsaturated disaccharides were calculated based on fluorescence intensity. Samples from sog9-ChGn-1-1 (■) and mock-transfected sog9 (□) cells are shown. Arrowheads indicate the size of molecular mass standards in kDa. Data represent one of a series of three independent experiments, and all three experiments gave essentially the same results.

however, overexpression of ChGn-1 increases CS levels in C4ST-1-deficient sog9 cells (see sog9-ChGn-1-1 and sog9-ChGn-1-2 cells in Table 3 in [26]). To further assess whether C4ST-1 was dispensable for regulating the number of CS chains synthesized by ChGn-1, the lengths of CS chains in sog9-ChGn-1-1-transfected and mock-transfected sog9 cells were compared. Gel-filtration analysis using a Superdex™ 200 column revealed that the length of CS chains in sog9-ChGn-1-1 cells was similar to that in mock-transfected cells (Figure 5). These results indicated that ChGn-1 regulated the number of CS chains without C4ST-1, and that C4ST-2 might play a key role in controlling the number of CS moieties synthesized by ChGn-1.

Introduction of C4ST-2 into L cells

We next examined whether C4ST-2 regulates the number of CS chains by preparing L cells in which C4ST-2 is overexpressed. The amount and disaccharide composition of CS isolated from two stable L cell clones that express different levels of C4ST-2 (high expression L-C4ST-2-1 and low expression L-C4ST-2-2 cells) were analysed by HPLC (Table 2). Although the disaccharide compositions of CS found in L-C4ST-2-1 and L-C4ST-2-2 cells were similar to those in control L cells, the levels of CS were higher in L-C4ST-2-1 and L-C4ST-2-2 cells; moreover, the CS levels corresponded to the C4ST-2 expression levels (Table 2).

We then determined whether knockdown of C4ST-2 decreased the amount of CS in L cells. The efficiency of gene silencing was determined by quantitative RT–PCR. Transfection with C4ST-2 shRNA (L-shRNA C4ST-2-1 or L-shRNA C4ST-2-2 cells: two different shRNAs targeted against C4ST-2 were used) resulted in a 70–80 % knockdown of *C4ST-2* mRNA and a 33–47 % decrease in the amount of CS when compared with control L cells. These results indicated that C4ST-2 regulated CS levels, and that CS levels were proportional to *C4ST-2* expression levels (Table 2).

Involvement of C4ST-2 in the increased number of CS chains

We next compared the lengths of CS chains in L-C4ST-2-1-, L-C4ST-2-2-, L-shRNA C4ST-2-1-, L-shRNA C4ST-2-2- and mock-transfected L cells. Gel-filtration analysis using a

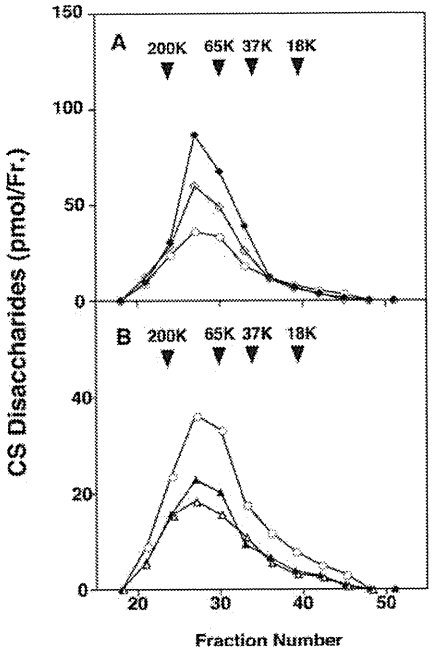

Figure 6 Analysis of the length of CS chains in L, L-C4ST-2, L-shRNA C4ST-2-1 and L-shRNA C4ST-2-2 cells

Purified CS fractions were subjected to reductive β-elimination using $NaBH_4$/NaOH and then analysed by gel-filtration chromatography on a Superdex™ 200 column (10 mm×300 mm). The digests of individual fractions obtained with chondroitinase ABC were derivatized with 2-aminobenzamide and then analysed by HPLC. The amounts of the 2-aminobenzamide derivatives of unsaturated disaccharides were calculated based on fluorescence intensity. (**A**) The samples from L-C4ST-2-1 (◆), L-C4ST-2-2 (◇) and mock-transfected L (○) cells are shown. (**B**) The samples from L-shRNA C4ST-2-1 (▲), L-shRNA C4ST-2-2 (△) and mock-transfected L (○) cells are shown. Arrowheads indicate the size of the molecular standards in kDa. Data represent one of a series of three independent experiments, and all three experiments gave essentially the same results.

Superdex™ 200 column revealed that the CS chain lengths in cells transfected with L-C4ST-2-1, L-C4ST-2-2, L-shRNA C4ST-2-1 or L-shRNA C4ST-2-2 were comparable with those in control L cells (Figures 6A and 6B), indicating that C4ST-2 regulated only the number of CS chains in L cells and that the number of CS chains corresponded to *C4ST-2* expression levels.

DISCUSSION

Previously, we have demonstrated that co-expression of any two of four ChSy family members, ChSy-1, ChSy-2, ChSy-3 and ChPF, promoted chondroitin polymerization with alternating GalNAc and GlcA residues on the linkage-region tetrasaccharide of α-TM [3–5]. These results indicated that ChGn-1 and ChGn-2, both of which have GalNAcT activity, were not required for chondroitin polymerization on the linkage-region tetrasaccharide. In fact, our recent studies found that knockdown of ChGn-2 resulted in a decrease in CS chain length and that ChGn-2 was involved in CS chain elongation [26]. In contrast with ChGn-2, ChGn-1-deficient mice had fewer CS chains in developing cartilage and a delayed cartilage development [20]. These results suggest that ChGn-1 is required for efficient initiation of CS chain polymerization; moreover, the presence of chondroitin polymerase, meaning any two of ChSy-1, ChSy-2, ChSy-3 and ChPF, does not compensate for the loss of ChGn-1. In addition, the number of CS chains on specific core proteins may be tightly regulated during cartilage development by temporal and spatial regulation of ChGn-1 expression, and progression of cartilage disease may result from defects in these regulatory systems.

Sakai et al. [27] reported that *in vitro* overexpression of ChGn-1 in chondrosarcoma cells increased the number of CS chains. Their observations, like ours, indicate that ChGn-1 regulates the initiation of CS. Nevertheless, the results of the present study indicated that chondroitin polymerization did not occur on the non-reducing terminal GalNAc-linkage structure (Figure 2, open squares). Interestingly, the non-reducing terminal GalNAc(4-*O*-sulfate)-linkage structure of CS was associated with an increased number of CS chains when the enzyme source was any one of several complexes that comprised any two of the four ChSy family (Figure 2). In addition, C4ST-2 efficiently transferred sulfate to the non-reducing terminal GalNAc-linkage residue (Figure 4). In conjunction with our previous findings, these results indicate that ChGn-1 co-operates with C4ST-2 to increase the number of CS moieties.

Notably, on the basis of the data in Figure 2, ChSy-1–ChSy-3 enzyme complexes seemed to play a central role in chondroitin polymerization on α-TM, although every ChSy complex tested polymerized chondroitin on α-TM. In our previous study, ChSy family members co-expressed in various combinations exhibited distinct but overlapping acceptor substrate specificities with two synthetic acceptor substrates, GlcAβ1-3Galβ1-*O*-naphthalenemethanol and GlcAβ1-3Galβ1-*O*-C_2H_4NH-benzyloxycarbonyl, both of which share a disaccharide sequence with the GAG–protein linkage region tetrasaccharide [4]. When using the two synthetic acceptor substrates, two complexes, ChSy-1–ChPF and ChSy-1–ChSy-3, polymerized more chondroitin than other complexes [4]. Moreover, we recently found that the non-reducing terminal 4-O-sulfation of GalNAc residues synthesized by C4ST-1 and ChGn-2 facilitated the elongation of CS chains only when the chondroitin polymerase comprised ChSy-1 and ChPF, and no polymerization was induced on these acceptors when ChSy-1 and ChSy-2, ChSy-1 and ChSy-3, ChSy-2 and ChSy-3, ChSy-2 and ChPF, or ChSy-3 and ChPF were co-expressed [26]. Furthermore, as shown in the present study, the non-reducing terminal GalNAc(4-*O*-sulfate)-linkage structure of CS was associated with an increase in the number of CS chains when any one of six ChSy complexes was the polymerase (Figure 2). Thus each ChSy complex may play a specific role in the biosynthesis of CS.

In the present study we propose that the chondroitin backbone was synthesized via two pathways (Figure 7). Pathway A shows that after synthesis of the linkage-region tetrasaccharide, the ChSy-1–ChSy-3 complex is primarily responsible for chondroitin polymerization. Pathway B shows that following complete synthesis of the linkage-region tetrasaccharide, ChGn-1 catalyses the transfer of a single GalNAc residue to the tetrasaccharide-linkage region and C4ST-2 then mediates the 4-O-sulfation of the non-reducing terminal GalNAc residue. Finally, the non-reducing terminal 4-O-sulfation of the GalNAc-linkage structure facilitated the elongation of CS chains via chondroitin polymerases that comprised any combination of two ChSy family members, although the chain lengths of chondroitin synthesized by different ChSy enzyme complexes differed (Figure 2). These results indicated that the mechanism of CS chain initiation, which is largely mediated by the ChGn-1 and C4ST-2, were similar to, but distinct from, the mechanisms of chain elongation, which was largely mediated by ChGn-2 and C4ST-1 [26].

In a previous study, it was shown that the synthesis of abnormally long CS chains that occurs during the development of atherosclerosis is accompanied by increases in expression

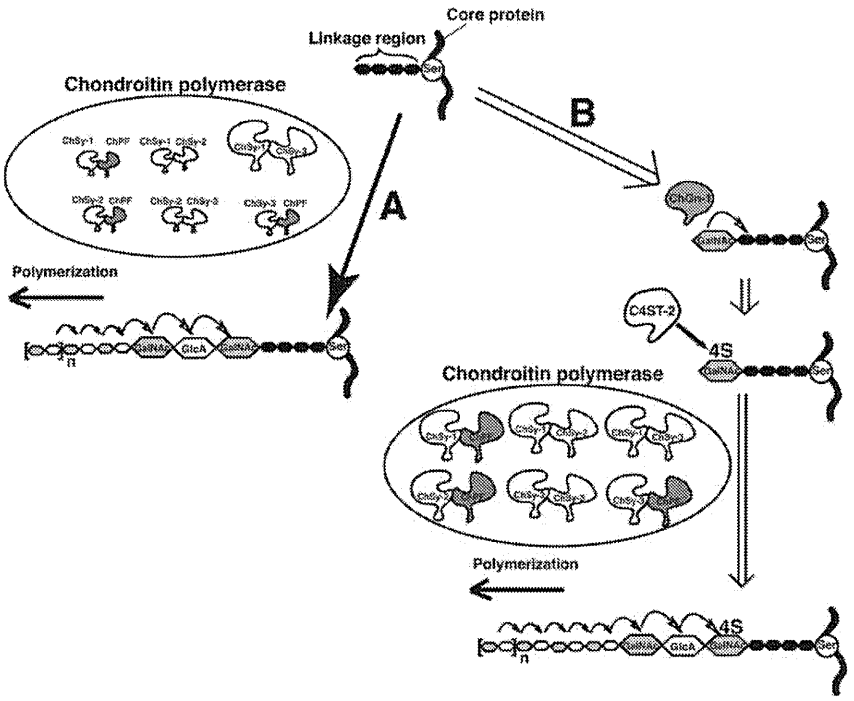

Figure 7 Mechanisms that increase the number of CS chains

CS is synthesized via two pathways. (**A**) Following complete synthesis of the linkage-region tetrasaccharide, chondroitin polymerization with alternating GalNAc and GlcA residues occurs by an enzyme complex comprising any two of four proteins: ChSy-1, ChSy-2, ChSy-3 and ChPF. (**B**) Following complete synthesis of the linkage-region tetrasaccharide, a single GalNAc residue is transferred to the tetrasaccharide-linkage region by ChGn-1, and C4ST-2 catalyses the 4-O-sulfation of the non-reducing terminal GalNAc residue. Finally, the non-reducing terminal 4-O-sulfation of the GalNAc-linkage structure facilitates the elongation of CS chains, which is catalysed by chondroitin polymerase consisting of any two of the following four proteins: ChSy-1, ChSy-2, ChSy-3 and ChPF.

of C4ST-1 and ChGn-2 [28]. In contrast, C4ST-2 and ChGn-1 expression levels do not change during the progression of atherosclerosis, suggesting that C4ST-2 and ChGn-1 may not be involved in CS chain elongation during the development of atherosclerosis [28]. These results indicate that functions of ChGn-1 and ChGn-2, or C4ST-1 and C4ST-2, are different, despite their overlapping substrate specificities *in vitro*. In addition, the C4ST-1–ChGn-2 and C4ST-2–ChGn-1 complexes are important in the regulation of CS chain length and the number of CS chains respectively. An analysis of ChGn-2- or C4ST-2-knockout mice should provide further insight into the distinct functions of these proteins. C4ST-2-knockout mice may exhibit a similar phenotype to ChGn-1-knockout mice.

ChGn-1-knockout mice had less cartilage than wild-type mice. Sato et al. [29] also indicated that ChGn-1-deficient mice exhibited slight dwarfism due to a minor impairment of endochondral ossification. These results suggest that ChGn-1 is required for normal cartilage development. To date, many of these cartilage deficiencies are characteristic of the degenerative alterations observed with OA (osteoarthritis). OA is a degenerative disease characterized by a loss of matrix CS and cartilage integrity [30]. A genome-wide gene expression analysis that compared human OA cartilage with normal donor cartilage identified an altered level of C4ST-1 expression in OA cartilage [31]. In fact, C4ST-1-knockout mice have severe cartilage defects, and are characterized by disorganized and hypercellular cartilage growth plates with a fibrillated ECM (extracellular matrix) and an overall loss of CS [32]. On the basis of the findings that both C4ST-1 and ChGn-1 play key roles in mammalian chondrocyte development and in the maintenance of healthy cartilage, it is likely that abnormal ChGn-1 and C4ST-2 expression may be involved in the pathogenic mechanisms of OA.

More recently, we found two missense mutations in the *ChGn-1* gene, and both were associated with a profound decrease in enzyme activity in two patients with neuropathy [33]. As we found in the present study, ChGn-1 regulated the chain number and amount of CS in these patients, which indicates that patients with neuropathies may suffer from decreased levels of CS. In addition, we demonstrated that ChGn-1 co-operates with C4ST-2 to increase the number of CS moieties. Thus C4ST-2 may also be associated with the pathogenesis of peripheral neuropathies because C4ST-2 abnormalities may inhibit recovery from minor trauma. Studies on larger numbers of patients and complete family studies are in progress.

AUTHOR CONTRIBUTION

Tomomi Izumikawa and Toshiyasu Koike performed the research, and Hiroshi Kitagawa designed the research. Tomomi Izumikawa and Hiroshi Kitagawa analysed the data. Tomomi Izumikawa and Hiroshi Kitagawa wrote the paper.

ACKNOWLEDGEMENT

We thank Professor Frank Tufaro (Allera Health Products, St. Petersburg, FL, U.S.A.) for providing the sog9 cells.

FUNDING

This work was supported, in part, by the Ministry of Health, Labor and Welfare of Japan [Health Sciences Research Grant on Psychiatric and Neurological Diseases and Mental

Health, grant number H21-012], and the Ministry of Education, Culture, Sports, Science and Technology (MEXT) [Grant-in-aid for Scientific Research, grant number B #21390025 (to H.K.) and Grant-in-aid for Scientific Research on Innovative Area (to H.K.)].

REFERENCES

1 Sugahara, K. and Kitagawa, H. (2000) Recent advances in the study of the biosynthesis and functions of sulfated glycosaminoglycans. Curr. Opin. Struct. Biol. **10**, 518–527
2 Kitagawa, H., Uyama, T. and Sugahara, K. (2001) Molecular cloning and expression of a human chondroitin synthase. J. Biol. Chem. **276**, 38721–38726
3 Izumikawa, T., Uyama, T., Okuura, Y., Sugahara, K. and Kitagawa, H. (2007) Involvement of chondroitin sulfate synthase-3 (chondroitin synthase-2) in chondroitin polymerization through its interaction with chondroitin synthase-1 or chondroitin polymerizing factor. Biochem. J. **403**, 545–552
4 Izumikawa, T., Koike, T., Shiozawa, S., Sugahara, K., Tamura, J. and Kitagawa, H. (2008) Identification of chondroitin sulfate glucuronyltransferase as chondroitin synthase-3 involved in chondroitin polymerization: chondroitin polymerization is achieved by multiple enzyme complexes consisting of chondroitin synthase family members. J. Biol. Chem. **283**, 11396–11406
5 Kitagawa, H., Izumikawa, T., Uyama, T. and Sugahara, K. (2003) Molecular cloning of a chondroitin polymerizing factor that cooperates with chondroitin synthase for chondroitin polymerization. J. Biol. Chem. **278**, 23666–23671
6 Uyama, T., Kitagawa, H., Tamura, J. and Sugahara, K. (2002) Molecular cloning and expression of human chondroitin *N*-acetylgalactosaminyltransferase: the key enzyme for chain initiation and elongation of chondroitin/dermatan sulfate on the protein linkage region tetrasaccharide shared by heparin/heparan sulfate. J. Biol. Chem. **277**, 8841–8846
7 Gotoh, M., Sato, T., Akashima, T., Iwasaki, H., Kameyama, A., Mochizuki, H., Yada, T., Inaba, N., Zhang, Y., Kikuchi, N. et al. (2002) Enzymatic synthesis of chondroitin with a novel chondroitin sulfate *N*-acetylgalactosaminyltransferase that transfers *N*-acetylgalactosamine to glucuronic acid in initiation and elongation of chondroitin sulfate synthesis. J. Biol. Chem. **277**, 38189–38196
8 Sato, T., Gotoh, M., Kiyohara, K., Akashima, T., Iwasaki, H., Kameyama, A., Mochizuki, H., Yada, T., Inaba, N., Togayachi, A. et al. (2003) Differential roles of two *N*-acetylgalactosaminyltransferases, CSGalNAcT-1, and a novel enzyme, CSGalNAcT-2. Initiation and elongation in synthesis of chondroitin sulfate. J. Biol. Chem. **278**, 3063–3071
9 Uyama, T., Kitagawa, H., Tanaka, J., Tamura, J., Ogawa, T. and Sugahara, K. (2003) Molecular cloning and expression of a second chondroitin *N*-acetylgalactosaminyltransferase involved in the initiation and elongation of chondroitin/dermatan sulfate. J. Biol. Chem. **278**, 3072–3078
10 Kusche-Gullberg, M. and Kjellén, L. (2003) Sulfotransferases in glycosaminoglycan biosynthesis. Curr. Opin. Struct. Biol. **13**, 605–611
11 Hiraoka, N., Nakagawa, H., Ong, E., Akama, T. O., Fukuda, M. N. and Fukuda, M. (2000) Molecular cloning and expression of two distinct human chondroitin 4-*O*-sulfotransferases that belong to the HNK-1 sulfotransferase gene family. J. Biol. Chem. **275**, 20188–20196
12 Kang, H.-G., Evers, M. R., Xia, G., Baenziger, J. U. and Schachner, M. (2002) Molecular cloning and characterization of chondroitin-4-O-sulfotransferase-3: a novel member of the HNK-1 family of sulfotransferases. J. Biol. Chem. **277**, 34766–34772
13 Evers, M. R., Xia, G., Kang, H.-G., Schachner, M. and Baenziger, J. U. (2001) Molecular cloning and characterization of a dermatan-specific *N*-acetylgalactosamine 4-*O*-sulfotransferase. J. Biol. Chem. **276**, 36344–36354
14 Yamauchi, S., Mita, S., Matsubara, T., Fukuta, M., Habuchi, H., Kimata, K. and Habuchi, O. (2000) Molecular cloning and expression of chondroitin 4-sulfotransferase. J. Biol. Chem. **275**, 8975–8981
15 Mikami, T., Mizumoto, S., Kago, N., Kitagawa, H. and Sugahara, K. (2003) Specificities of three distinct human chondroitin/dermatan *N*-acetylgalactosamine 4-*O*-sulfotransferases demonstrated using partially desulfated dermatan sulfate as an acceptor: implication of differential roles in dermatan sulfate biosynthesis. J. Biol. Chem. **278**, 36115–36127
16 Fukuta, M., Uchimura, K., Nakashima, K., Kato, M., Kimata, K., Shinomura, T. and Habuchi, O. (1995) Molecular cloning and expression of chick chondrocyte chondroitin 6-sulfotransferase. J. Biol. Chem. **270**, 18575–18580
17 Tsutsumi, K., Shimakawa, H., Kitagawa, H. and Sugahara, K. (1998) Functional expression and genomic structure of human chondroitin 6-sulfotransferase. FEBS Lett. **441**, 235–241
18 Kobayashi, M., Sugumaran, G., Liu, J., Shworak, N. W., Silbert, J. E. and Rosenberg, R. D. (1999) Molecular cloning and characterization of a human uronyl 2-sulfotransferase that sulfates iduronyl and glucuronyl residues in dermatan/chondroitin sulfate. J. Biol. Chem. **274**, 10474–10480
19 Ohtake, S., Ito, Y., Fukuta, M. and Habuchi, O. (2001) Functional expression and genomic structure of human chondroitin 6-sulfotransferase. J. Biol. Chem. **276**, 43894–43900
20 Watanabe, Y., Takeuchi, K., Higa-Onaga, S., Tsujita, M., Abe, M., Natsume, R., Li, M., Furuichi, T., Saeki, M., Izumikawa, T. et al. (2010) Chondoroitin sulfate *N*-acetylgalactosaminyltransferase-1 is required for normal cartilage development. Biochem. J. **432**, 47–55
21 Nawa, K., Sakano, K., Fujiwara, H., Sato, Y., Sugiyama, N., Teruuchi, T., Iwamoto, M. and Marumoto, Y. (1990) Presence and function of chondroitin-4-sulfate on recombinant human soluble thrombomodulin. Biochem. Biophys. Res. Commun. **171**, 729–737
22 Nadanaka, S., Kitagawa, H. and Sugahara, K. (1998) Demonstration of the immature glycosaminoglycan tetrasaccharide sequence GlcAβ1-3Galβ1-3Galβ1-4Xyl on recombinant soluble human α-thrombomodulin. An oligosaccharide structure on a 'part-time' proteoglycan. J. Biol. Chem. **273**, 33728–33734
23 Uyama, T., Ishida, M., Izumikawa, T., Trybala, E., Tufaro, F., Bergström, T., Sugahara, K. and Kitagawa, H. (2006) Chondroitin 4-*O*-sulfotransferase-1 regulates E disaccharide expression of chondroitin sulfate required for herpes simplex virus infectivity. J. Biol. Chem. **281**, 38668–38674
24 Kinoshita, A. and Sugahara, K. (1999) High-performance liquid chromatography: application to disaccharide composition analysis and exosequencing of oligosaccharides. Anal. Biochem. **269**, 367–378
25 Koike, T., Izumikawa, T., Tamura, J. and Kitagawa, H. (2009) FAM20B is a kinase that phosphorylates xylose in the glycosaminoglycan-protein linkage region. Biochem. J. **421**, 157–162
26 Izumikawa, T., Okuura, Y., Koike, T., Sakoda, N. and Kitagawa, H. (2011) Chondroitin 4-*O*-sulfotransferase-1 regulates the chain length of chondroitin sulfate in co-operation with chondroitin *N*-acetylgalactosaminyltransferase-2. Biochem. J. **434**, 321–331
27 Sakai, K., Kimata, K., Sato, T., Gotoh, M., Narimatsu, H., Shinomiya, K. and Watanabe, H. (2007) Chondroitin sulfate *N*-acetylgalactosaminyltransferase-1 plays a critical role in chondroitin sulfate synthesis in cartilage. J. Biol. Chem. **282**, 4152–4161
28 Anggraeni, V. Y., Emoto, N., Yagi, K., Mayasari, D. S., Nakayama, K., Izumikawa, T., Kitagawa, H. and Hirata, K. (2011) Correlation of C4ST-1 and ChGn-2 expression with chondroitin sulfate chain elongation in atherosclerosis. Biochem Biophys. Res. Commun. **406**, 36–41
29 Sato, T., Kudo, T., Ikehara, Y., Ogawa, H., Hirano, T., Kiyohara, K., Hagiwara, K., Togayachi, A., Ema, M., Takahashi, S. et al. (2011) Chondroitin sulfate *N*-acetylgalactosaminyltransferase 1 is necessary for normal endochondral ossification and aggrecan metabolism. J. Biol. Chem. **286**, 5803–5812
30 Krasnokutsky, S., Samuels, J. and Abramson, S. B. (2007) Osteoarthritis in 2007. Bull. NYU. Hosp. Jt. Dis. **65**, 222–228
31 Karlsson, C., Dehne, T., Lindahl, A., Brittberg, M., Pruss, A. and Sittinger, M. (2010) Genome-wide expression profiling reveals new candidate genes associated with osteoarthritis. Osteoarthritis Cartilage **18**, 581–592
32 Kluppel, M., Wight, T. N., Chan, C., Hinek, A. and Wrana, J. L. (2005) Maintenance of chondroitin sulfation balance by chondroitin-4-sulfotransferase 1 is required for chondrocyte development and growth factor signaling during cartilage morphogenesis. Development **132**, 3989–4003
33 Saigoh, K., Izumikawa, T., Koike, T., Shimizu, J., Kitagawa, H. and Kusunoki, S. (2011) Chondroitin β1,4-*N*-acetylgalactosaminyltransferase-1 missense mutations are associated with neuropathies. J. Hum. Genet. **56**, 143–146

Received 11 August 2011/19 September 2011; accepted 27 September 2011
Published as BJ Immediate Publication 27 September 2011, doi:10.1042/BJ20111472

nature neuroscience

Persistent cortical plasticity by upregulation of chondroitin 6-sulfation

Shinji Miyata[1,2], Yukio Komatsu[3], Yumiko Yoshimura[4], Choji Taya[5] & Hiroshi Kitagawa[1,2]

Cortical plasticity is most evident during a critical period in early life, but the mechanisms that restrict plasticity after the critical period are poorly understood. We found that a developmental increase in the 4-sulfation/6-sulfation (4S/6S) ratio of chondroitin sulfate proteoglycans (CSPGs), which are components of the brain extracellular matrix, leads to the termination of the critical period for ocular dominance plasticity in the mouse visual cortex. Condensation of CSPGs into perineuronal nets that enwrapped synaptic contacts on parvalbumin-expressing interneurons was prevented by cell-autonomous overexpression of chondroitin 6-sulfation, which maintains a low 4S/6S ratio. Furthermore, the increase in the 4S/6S ratio was required for the accumulation of Otx2, a homeoprotein that activates the development of parvalbumin-expressing interneurons, and for functional maturation of the electrophysiological properties of these cells. Our results indicate that the critical period for cortical plasticity is regulated by the 4S/6S ratio of CSPGs, which determines the maturation of parvalbumin-expressing interneurons.

Ocular dominance plasticity is a classic example that has been used to study the effects of experience on cortical circuits[1,2]. Brief monocular deprivation leads to a reduction in the responses of visual cortical neurons to the deprived eye and an increase in the responses to the nondeprived eye. Sensitivity to monocular deprivation is high in juvenile animals during a critical period in early life (postnatal days 19–32 (P19–32) in the mouse visual cortex), after which cortical neurons become less plastic[3]. Considerable evidence indicates that functional changes in the balance between excitation and inhibition control ocular dominance plasticity[2]. In particular, maturation of a subset of inhibitory interneurons expressing the calcium-binding protein parvalbumin has been proposed to be crucial for defining the timing of the critical period[2,4,5].

CSPGs consist of a core protein with covalently attached chondroitin sulfate glycosaminoglycan chains (**Fig. 1a**) and are major components of the brain extracellular matrix[6]. During postnatal development, CSPGs condense around the soma and proximal dendrites of parvalbumin-expressing interneurons, forming perineuronal nets (PNNs), a specialized extracellular matrix structure that interdigitates with synaptic contacts[7]. PNNs are composed of several CSPGs and hyaluronan, and the interaction between CSPGs and hyaluronan is stabilized by tenascin-R and cartilage link proteins[8]. Although the cellular origins of their components are not fully understood, both neurons and glial cells may contribute to the formation of PNNs[9]. Digestion of chondroitin sulfate chains with chondroitinase ABC disrupts PNNs and reactivates ocular dominance plasticity in adult animals after the closure of the critical period, indicating that the chondroitin sulfate moieties of CSPGs are responsible for PNN formation and control of the critical period plasticity[10]. It has been suggested that chondroitin sulfate chains present a physical barrier that limits the critical period plasticity by preventing rearrangements of synaptic connections because they inhibit axonal sprouting and regeneration after nerve injury[11]. However, it is unlikely that all chondroitin sulfate chains inherently inhibit plasticity, as chondroitin sulfate chains are very abundant, even in the juvenile brain during the critical period.

Recent studies have proposed that the functional information of CSPGs is encoded by the specific sulfation sequence of chondroitin sulfate chains[6,12–14]. Chondroitin sulfate chains are long linear polysaccharides that are composed of a repeating disaccharide unit that consists of glucuronic acid and *N*-acetylgalactosamine (GalNAc)[6]. During biosynthesis, GalNAc residues of the repeating disaccharide units are sulfated at C6 and C4 by chondroitin 6-sulfotransferase-1 (C6ST-1) and chondroitin 4-sulfotransferase-1 (C4ST-1), respectively (**Fig. 1a**). Chondroitin sulfate chains can act as both inhibitory molecules for axonal growth and neuritogenic molecules depending on their sulfation status[6,13]. Previously, we found that the neuritogenic effect of particular chondroitin sulfate chains was mediated by specific interaction with a cell adhesion molecule, contactin-1 (ref. 13). Despite increasing *in vitro* evidence that chondroitin sulfate chains act in a sulfation pattern–dependent manner, the role of CSPG sulfation patterns in cortical plasticity has garnered little attention. Specifically, the relationship between sulfation patterns of chondroitin sulfate and functional maturation of inhibitory interneurons has not been addressed. Moreover, the importance of specific sulfation patterns of chondroitin sulfate to cortical plasticity may have been overlooked in previous studies of chondroitin sulfate and plasticity because chondroitinase ABC treatment destroys all chondroitin

[1]Department of Biochemistry, Kobe Pharmaceutical University, Higashinada-ku, Kobe, Japan. [2]Global Center of Excellence Program for Signal Transduction Medicine, Graduate School of Medicine, Kobe University, Chuo-ku, Kobe, Japan. [3]Department of Neuroscience, Research Institute of Environmental Medicine, Nagoya University, Nagoya, Japan. [4]Division of Developmental Neurophysiology, Okazaki Institute for Integrative Bioscience (National Institute for Physiological Sciences), National Institutes for Natural Sciences, Okazaki, Japan. [5]Laboratory for Transgenic Technology, The Tokyo Metropolitan Institute of Medical Science, Tokyo, Japan. Correspondence should be addressed to H.K. (kitagawa@kobepharma-u.ac.jp).

Received 3 October 2011; accepted 6 December 2011; published online 15 January 2012; doi:10.1038/nn.3023

sulfate chains, irrespective of sulfation status. The 4S/6S ratio changes during several biological processes[15,16]; thus, we hypothesized that sulfation patterns of chondroitin sulfate regulate the critical period plasticity. To test this hypothesis, we generated transgenic mice that overexpress human C6ST-1, a sulfotransferase catalyzing the 6-sulfation of chondroitin sulfate chains, under the control of a chicken β-actin promoter.

RESULTS

Sulfation patterns of chondroitin sulfate in mouse brain

We initially examined sulfation patterns of chondroitin sulfate in the developing mouse brain. Chondroitin sulfate chains isolated from mouse brain at different ages were digested with chondroitinase ABC and the resultant disaccharides were analyzed by high-performance liquid chromatography (**Supplementary Table 1**). In wild-type mice, the proportion of chondroitin 6-sulfation gradually decreased, whereas that of chondroitin 4-sulfation progressively increased (**Fig. 1b,c**), which resulted in a sharp increase in the 4S/6S ratio during development (**Fig. 1d**). In adult wild-type brain, chondroitin sulfate chains were mostly composed of chondroitin 4-sulfation, with chondroitin 6-sulfation only accounting for 2% of the total chondroitin sulfate. *C6ST-1* (also known as *CHST3*) transgenic mice showed an increased proportion of chondroitin 6-sulfation and a decreased proportion of chondroitin 4-sulfation throughout development relative to control mice. The 4S/6S ratio in *C6ST-1* transgenic mice was substantially lower than the ratio in control mice from P14 onward. Although the sulfation patterns of chondroitin sulfate changed markedly, the total amount of chondroitin sulfate remained constant during development and did not differ between *C6ST-1* transgenic and wild-type mice (**Fig. 1e**).

We also found that the developmental shift of the 4S/6S ratio correlated with the maturation timing of cortical regions. The 4S/6S ratio shift in the visual cortex occurred after that in the somatosensory cortex (**Fig. 1f**), which is consistent with the later maturation of the visual cortex[17]. Raising animals in complete darkness (dark rearing) delays the onset and termination of the critical period for ocular dominance plasticity in the visual cortex[2]. However, the 4S/6S ratio in the visual cortex was not affected by dark rearing (control, $n = 4$, 4S/6S ratio = 16.8 ± 0.39; dark rearing, $n = 4$, 4S/6S ratio = 15.9 ± 0.30; $P > 0.1$), suggesting that the temporal shift of the 4S/6S ratio is developmentally programmed, but is not dependent on visual experience. On the basis of immunohistochemical analysis using CS56 antibody that recognizes chondroitin 6-sulfation–related structures[18], we found that the shift in the sulfation patterns of chondroitin sulfate in *C6ST-1* transgenic mice was delayed relative to that in wild-type mice (**Fig. 1g**), which is consistent with the results of our chemical disaccharide composition analysis. These results indicate that the sulfation patterns, but not the amount of chondroitin sulfate chains, changed during the critical period and that *C6ST-1* transgenic mice retain immature sulfation patterns of chondroitin sulfate throughout life.

C6ST-1 transgenic adults retain ocular dominance plasticity

To investigate whether the sulfation patterns of chondroitin sulfate influence the onset of the critical period, we assessed ocular dominance

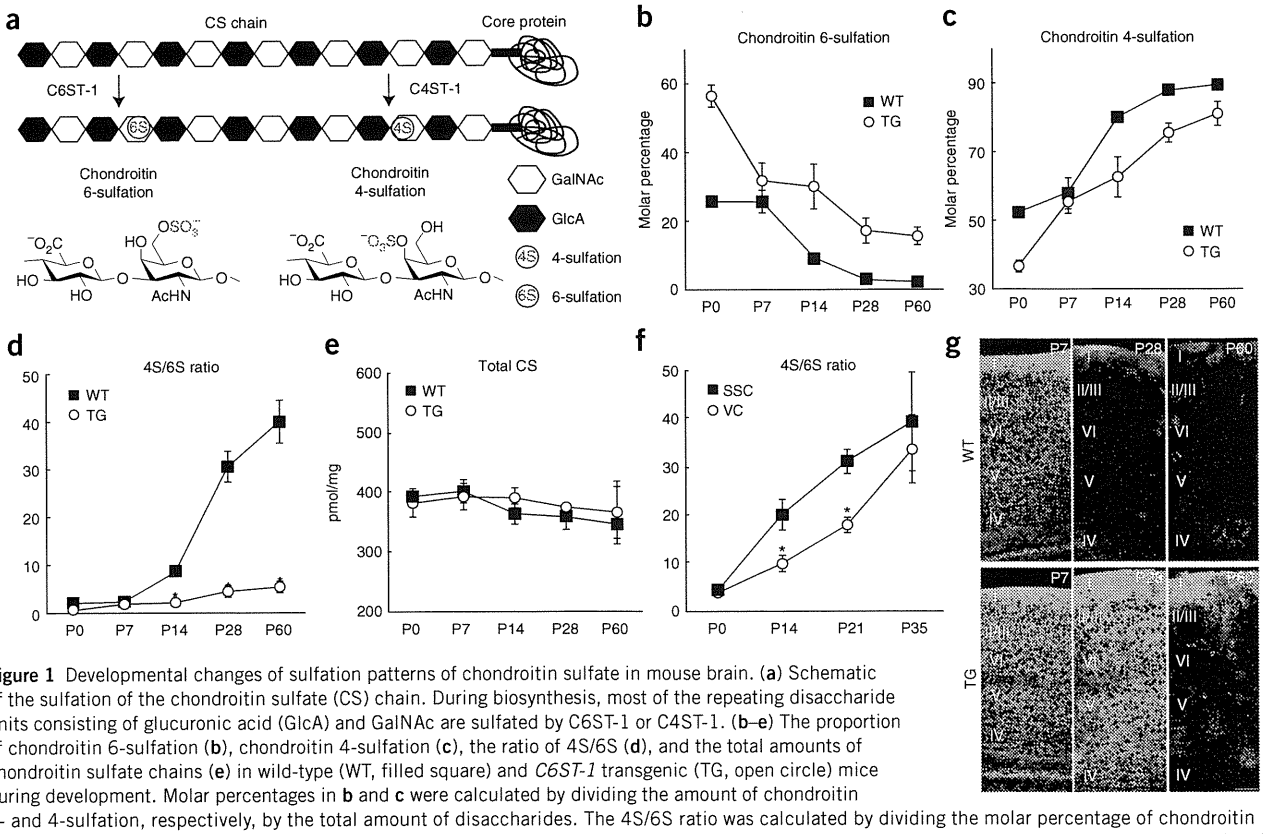

Figure 1 Developmental changes of sulfation patterns of chondroitin sulfate in mouse brain. (**a**) Schematic of the sulfation of the chondroitin sulfate (CS) chain. During biosynthesis, most of the repeating disaccharide units consisting of glucuronic acid (GlcA) and GalNAc are sulfated by C6ST-1 or C4ST-1. (**b–e**) The proportion of chondroitin 6-sulfation (**b**), chondroitin 4-sulfation (**c**), the ratio of 4S/6S (**d**), and the total amounts of chondroitin sulfate chains (**e**) in wild-type (WT, filled square) and *C6ST-1* transgenic (TG, open circle) mice during development. Molar percentages in **b** and **c** were calculated by dividing the amount of chondroitin 6- and 4-sulfation, respectively, by the total amount of disaccharides. The 4S/6S ratio was calculated by dividing the molar percentage of chondroitin 4-sulfation by that of chondroitin 6-sulfation. (**f**) The ratio of 4S/6S in the somatosensory cortex (SSC, filled square) and visual cortex (VC, open circle) in wild-type mice. Error bars represent s.d. ($n = 3$ for each point). *$P < 0.05$ (Student's t test) between the two groups at the same time point. (**g**) *C6ST-1* transgenic mice showed a delayed decrease in CS56 staining in the developing visual cortex. Cortical layers are indicated with Roman numerals on the left. Scale bar represents 100 μm.

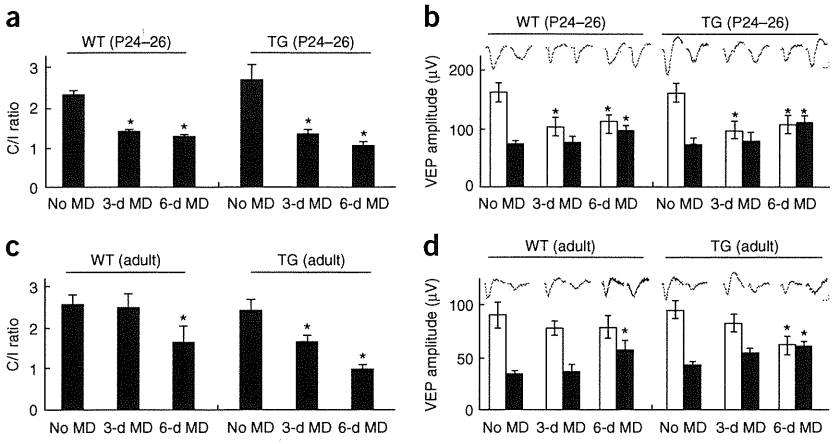

Figure 2 Sulfation patterns of chondroitin sulfate participate in the termination of the critical period. (**a**) Monocular deprivation periods of 3 or 6 d beginning at P24–26 resulted in a significant decrease in the contralateral/ipsilateral (C/I) ratio in both wild-type and *C6ST-1* mice as compared with nondeprived (No MD) mice. (**b**) In both groups, 3-d monocular deprivation depressed responses to the deprived eye (open bars) and 6-d monocular deprivation potentiated responses to the nondeprived eye (filled bars) (No MD: wild type $n = 12$, *C6ST-1*, $n = 10$; 3-d monocular deprivation: wild type $n = 18$, *C6ST-1*, $n = 14$; 6-d monocular deprivation: wild type $n = 12$, *C6ST-1*, $n = 11$). (**c**) In adulthood (P60–90), 3-d monocular deprivation did not affect the contralateral/ipsilateral ratio in wild-type mice, but did induce a significant contralateral/ipsilateral shift in *C6ST-1* mice. 6 d of monocular deprivation caused a significant contralateral/ipsilateral shift in both groups. (**d**) In wild-type mice, 6-d monocular deprivation induced potentiation of the responses to the nondeprived eye (filled bars), but no change in the responses to the deprived eye (open bars). *C6ST-1* mice showed depression in the responses to the deprived eye and potentiation of the responses to nondeprived eye (No MD: wild type $n = 11$, *C6ST-1*, $n = 12$; 3-d monocular deprivation: wild type $n = 10$, *C6ST-1*, $n = 11$; 6-d monocular deprivation: wild type $n = 8$, *C6ST-1*, $n = 14$). $^*P < 0.05$ (Student's t test) from No MD groups. Error bars represent s.e.m. Representative waveforms of VEPs are shown at the top of **b** and **d**. Scale bars represent 100 ms and 100 μV.

plasticity by recording visual evoked potentials (VEPs) from the binocular zone of the primary visual cortex. In both groups, the baseline ratio of contralateral eye VEP amplitude to ipsilateral eye VEP amplitude (the contralateral/ipsilateral ratio) was approximately 2, reflecting the contralateral eye dominance (**Fig. 2a**). We found that a 3- or 6-d monocular deprivation from P24–26 (the peak of the critical period) resulted in a significantly decreased contralateral/ipsilateral ratio in both groups ($P < 0.05$; **Fig. 2a**). Comparison of VEP amplitudes before and after monocular deprivation revealed two temporally distinct mechanisms for ocular dominance shift, as have been reported previously[19]. In both groups, the decrease in the contralateral/ipsilateral ratio was mediated by rapid depression of the responses to the deprived eye and by delayed potentiation of the responses to the nondeprived eye (**Fig. 2b**). Eye-specific projections from the retina to the dorsal lateral geniculate nucleus (dLGN) are known to be established in the first postnatal week[20]. *C6ST-1* transgenic mice had normal eye-specific segregation of retinogeniculate axon terminals in the dLGN (**Supplementary Fig. 1**). Together, these results suggest that the initial construction of visual pathway and the onset of the critical period occur normally in *C6ST-1* transgenic mice.

We next explored the effect of an altered sulfation pattern of chondroitin sulfate on the termination of the critical period. A 3-d monocular deprivation period did not alter the contralateral/ipsilateral ratio in wild-type adults as it had in juvenile mice (**Fig. 2c**). However, *C6ST-1* transgenic adults did experience a significant contralateral/ipsilateral shift ($P = 0.02$) following 3 d of monocular deprivation imposed after the critical period. Although recent studies have suggested that a longer period of monocular deprivation can induce a weak shift in the contralateral/ipsilateral ratio in adult animals, the nature of juvenile and adult ocular dominance plasticity is markedly different[21]. In wild-type adults, 6 d of monocular deprivation caused a mild, but statistically significant ($P < 0.05$), contralateral/ipsilateral shift that was mainly mediated by increased responses to the nondeprived eye, rather than by decreased responses to the deprived eye (**Fig. 2d**). This indicates that depression in responses to the deprived eye in wild-type mice is restricted to the critical period. In contrast, the contralateral/ipsilateral shift in *C6ST-1* transgenic adults caused by 6 d of monocular deprivation resulted from both depression in responses to the deprived eye and potentiation of responses to the nondeprived eye, which is similar to that observed in juvenile mice. These results suggest that *C6ST-1* transgenic adults retain juvenile-like ocular dominance plasticity.

C6ST-1 transgenic mice have reduced PNNs formation

We next examined whether the sulfation patterns of chondroitin sulfate affected formation of PNNs using a well-established marker, *Wisteria floribunda* agglutinin (WFA)[22]. During the first postnatal week, CSPGs were diffusely distributed and no PNN was observed in the visual cortex (**Fig. 3**). Formation of WFA$^+$ PNNs began around P14, gradually increased after the critical period and displayed a time course similar to the shift in the 4S/6S ratio (**Fig. 3a,b**). In the visual cortex of wild-type adults, most parvalbumin-expressing interneurons (90%) were surrounded by WFA$^+$ PNNs. Notably, *C6ST-1* transgenic mice showed a significantly reduced ($P = 0.002$ for P28, $P = 0.0005$ for adults) number of WFA$^+$ PNNs during and after the critical period (**Fig. 3a,c**); however, the number of parvalbumin-expressing interneurons was similar in wild-type and *C6ST-1* transgenic mice (**Fig. 3a,d**). This indicates that developmental changes in sulfation patterns of chondroitin sulfate are required for normal formation of PNNs.

Notably, some parvalbumin-expressing interneurons (10%) in *C6ST-1* transgenic mice were enwrapped by a distinct PNN-like structure that was recognized by CS56 antibody (**Fig. 3e**). These CS56$^+$ PNNs rarely colocalized with conventional WFA$^+$ PNNs in *C6ST-1* transgenic mice and were not observed in wild-type controls (**Fig. 3f**). Thus, the lack of WFA staining does not necessarily mean the absence of PNNs in *C6ST-1* transgenic mice. Instead, subpopulation of parvalbumin-expressing interneurons was surrounded by chondroitin 6-sulfation–enriched PNNs. Western blot analysis showed that the overall quantity of various core proteins, including aggrecan, a major CSPG in PNNs[23], were not altered in *C6ST-1* transgenic mice (**Supplementary Fig. 2**), indicating that abnormal formation of PNNs in *C6ST-1* transgenic mice is not a result of the reduced expression of PNN components. These results indicate that overexpression of C6ST-1 reduces the formation of conventional WFA$^+$ PNNs and increases the number of CS56$^+$ PNNs rich in chondroitin 6-sulfation around parvalbumin-expressing interneurons.

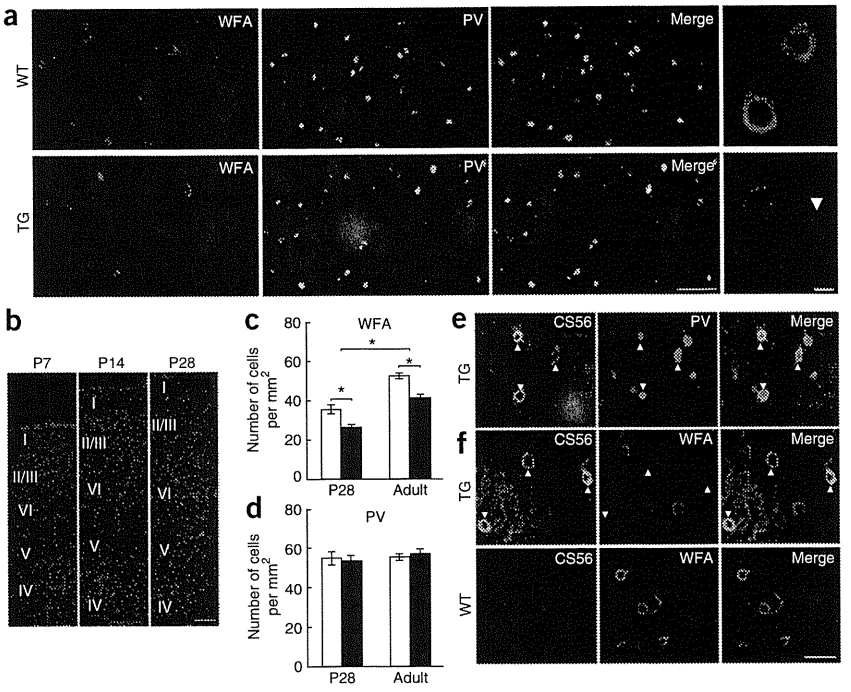

Figure 3 Impaired PNNs formation in *C6ST-1* mice. (**a**) Adult *C6ST-1* mice showed decreased formation of WFA$^+$ PNNs relative to controls. Right, high-magnification images of parvalbumin (PV)-expressing interneurons with or without (arrowhead) WFA$^+$ PNNs. (**b**) WFA$^+$ PNNs (red) first appeared at P14 in the visual cortex of wild-type mice. Nuclei were counterstained with Hoechst (blue). Cortical layers are indicated with Roman numerals on the left. (**c**,**d**) The number of WFA$^+$ PNNs (**c**), but not parvalbumin-expressing interneurons (**d**) in *C6ST-1* mice (closed bars) was significantly less than controls (open bars) throughout life. $^*P < 0.005$ (Student's *t* test) between control versus *C6ST-1* transgenic for P28 and adult (P60–90), and P28 versus adult for control and *C6ST-1* transgenic. Error bars represent s.e.m.; $n = 4$–9. (**e**) Subpopulation of parvalbumin-expressing interneurons were surrounded by chondroitin 6-sulfation–enriched CS56$^+$ PNNs (arrowheads) in *C6ST-1* mice. (**f**) CS56$^+$ PNNs (arrowheads) were not colocalized with conventional WFA$^+$ PNNs in *C6ST-1* mice and were not observed in wild-type mice. Scale bars represent 100 μm (left panels in **a**,**b**), 10 μm (right panels in **a**) and 50 μm (**e**,**f**).

Sulfation patterns of PNNs regulate accumulation of Otx2

How could the sulfation patterns of chondroitin sulfate in PNNs influence critical period plasticity? The Otx2 homeoprotein was recently shown to regulate ocular dominance plasticity via its effects on maturation of parvalbumin-expressing interneurons[5]. Previous data suggest that Otx2 protein produced in the retina and dLGN is transported to the visual cortex via thalamocortical axons, secreted from thalamocortical terminals and internalized by postsynaptic parvalbumin-expressing interneurons[5]. However, because less than 20% of all thalamocortical synapses contact inhibitory interneurons, including parvalbumin-expressing interneurons[24], it is unclear how Otx2 selectively accumulates in parvalbumin-expressing interneurons. Thus, we tested whether the sulfation patterns of PNNs around parvalbumin-expressing interneurons affect the incorporation of Otx2. In the visual cortex of wild-type mice, Otx2 protein first became evident in parvalbumin-expressing interneurons during the critical period, and the number of Otx2$^+$ cell was substantially increased by adulthood (**Fig. 4a**,**b**). Notably, there were significantly fewer ($P = 0.001$ for P28, $P = 0.0002$ for adults) Otx2$^+$ cells in *C6ST-1* transgenic mice than in wild-type mice (**Fig. 4a**,**b**). Otx2 was mostly detected in parvalbumin-expressing interneurons surrounded by WFA$^+$ PNNs, but was not observed in parvalbumin-expressing interneurons surrounded by CS56$^+$ PNNs (**Fig. 4c**), suggesting that the accumulation of Otx2 was dependent on the sulfation patterns of chondroitin sulfate in PNNs. Closer observation revealed that Otx2 was distributed in a punctate pattern in the soma and proximal dendrites of parvalbumin-expressing interneuron (**Fig. 4d**). Otx2-immnopositive puncta did not overlap with, but were closely apposed to, WFA$^+$ PNNs. The expression of *Otx2* mRNA in the retina and dLGN was indistinguishable between the two groups, excluding the possibility that overexpression of C6ST-1 affects expression of *Otx2* transcripts (**Supplementary Fig. 3**). Neither wild-type nor *C6ST-1* transgenic mice expressed detectable levels of *Otx2* mRNA in the visual cortex.

We further analyzed the spatial relationship between PNNs and thalamocortical synaptic contact sites in layer 4, which receives most of the thalamocortical input. Three-dimensional reconstruction of WFA$^+$ PNNs revealed a distinct meshwork surrounding soma and proximal dendrites of parvalbumin-expressing interneurons in wild-type mice (**Fig. 5a**). We selectively labeled thalamocortical boutons using antibody against vesicular glutamate transporter 2 (VGluT2)[24]. The holes in the meshwork of WFA$^+$ PNNs were evidently the areas occupied by thalamocortical boutons. In contrast, CS56$^+$ PNNs showed sparse dot-like particles rather than a meshwork structure, and thalamocortical boutons projecting onto parvalbumin-expressing interneurons in *C6ST-1* transgenic mice were not surrounded by PNNs (**Fig. 5a**). Because both WFA lectin and CS56 antibody recognize the chondroitin sulfate moiety of CSPGs, we stained WFA$^+$ and CS56$^+$ PNNs with an antibody recognizing the core protein portion of aggrecan. This confirmed the meshwork structure of WFA$^+$ PNNs in controls and the diffusely spread and less condensed morphology of CS56$^+$ PNNs in *C6ST-1* transgenic mice (**Fig. 5b**). These results indicate that diffuse PNNs that are rich in chondroitin 6-sulfation may be unable to tightly surround thalamocortical synaptic contacts, leading to diffusion and reduced accumulation of Otx2 at these contacts.

Overexpression of C6ST-1 in inhibitory interneurons

To address the cellular origin of the abnormal PNNs formation in *C6ST-1* transgenic mice, we carried out two series of experiments. First, we assessed the possible contribution of astrocytes to the formation of CS56$^+$ PNNs using a heterologous neuron and astrocyte coculture system. We found that parvalbumin-expressing interneurons were surrounded by CS56$^+$ PNNs when cortical neurons from *C6ST-1* transgenic, but not wild type, mice were grown on an astrocyte monolayer, regardless of the origin of the astrocytes (**Supplementary Fig. 4**). This suggests that overexpression of C6ST-1 in neurons, but not in astrocytes, is required for the formation of CS56$^+$ PNNs.

Second, we sought to directly determine whether cell-autonomous upregulation of chondroitin 6-sulfation in parvalbumin-expressing interneurons induces the formation of CS56$^+$ PNNs *in vivo*. In contrast with excitatory pyramidal neurons that are born in the

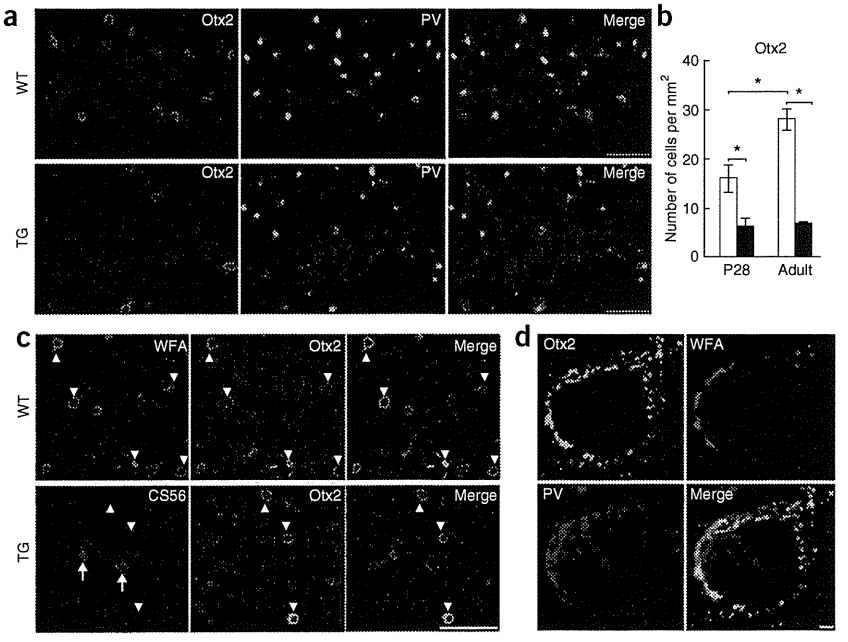

Figure 4 Sulfation patterns of chondroitin sulfate–dependent accumulation of Otx2 homeoprotein in parvalbumin-expressing interneurons. (**a**) In adult visual cortex, *C6ST-1* mice had reduced accumulation of Otx2 in parvalbumin-expressing interneurons as relative to controls. (**b**) Quantitative analysis of the number of Otx2$^+$ cells in wild-type (open bars) and *C6ST-1* (closed bars) mice. $^*P < 0.05$ (Student's *t* test) between P28 versus adult for control and control versus *C6ST-1* transgenic for P28 and adult. Error bars represent s.e.m. ($n = 3$–6). (**c**) Otx2 (arrowheads) accumulated in parvalbumin-expressing interneurons surrounded by WFA$^+$ PNNs in controls, but not in parvalbumin-expressing interneurons surrounded by CS56$^+$ PNNs (arrows) in *C6ST-1* mice. (**d**) Otx2-immnopositive puncta in parvalbumin-expressing interneurons closely apposed to WFA$^+$ PNNs. Scale bars represent 100 μm (**a**,**c**) and 2 μm (**d**).

cortical proliferative zones, inhibitory interneurons, including parvalbumin-expressing interneurons, originate from the ganglionic eminences and migrate tangentially into the cortex[25]. Thus, to achieve interneuron-specific gene expression, we performed ganglionic eminence–directed *in utero* electroporation[26,27] with *C6ST-1*–expressing and *yellow fluorescence protein* (*YFP*)-expressing plasmids at embryonic day 12.5 (E12.5; **Fig. 6a**). Immunohistochemical analysis of the postnatal cortex at P30 showed that 26% of transfected neurons ($n = 24$ of 91 YFP-positive neurons) were immunoreactive for parvalbumin (**Fig. 6b**). Notably, in contrast with untransfected control parvalbumin-expressing interneurons, most C6ST-1–transfected parvalbumin-expressing interneurons were surrounded by CS56$^+$ PNNs (88%, $n = 21$ of 24 YFP and parvalbumin double-positive neurons; **Fig. 6b**). As observed in *C6ST-1* transgenic mice, Otx2 was not accumulated in parvalbumin-expressing interneurons surrounded by CS56$^+$ PNNs (0%, $n = 0$ of 20 YFP and CS-56 double-positive neurons; **Fig. 6c**). No CS56$^+$ PNNs were formed when C6ST-1 was overexpressed in excitatory pyramidal neurons (**Fig. 6d**). These results indicate that PNNs formation and Otx2 accumulation were locally affected by parvalbumin-expressing interneuron autonomous production of chondroitin 6-sulfation. In addition, these results suggest that sulfation patterns of chondroitin sulfate are involved in the uptake of Otx2 at the postsynaptic level, but not at the presynaptic level (for example, transport from subcortical to cortical areas and secretion from presynaptic terminals).

Electrophysiological properties of visual cortical neurons

We then asked what kinds of changes are produced in the electrophysiological properties of parvalbumin-expressing interneurons by overexpression of C6ST-1 using slice preparations of visual cortex at P30–34, after the peak of ocular dominance plasticity. Whole-cell recordings were conducted from nonpyramidal neurons located in or near layer 4 with patch pipettes containing biocytin in the current-clamp mode. We analyzed fast-spiking cells, as parvalbumin-expressing interneurons are practically equivalent to fast-spiking cells[28]. We encountered cells showing spike discharges that were characteristic of fast-spiking cells in *C6ST-1* transgenic, as well as in wild-type, mice. A relative lack of spike-frequency adaptation during repetitive firing, a characteristic

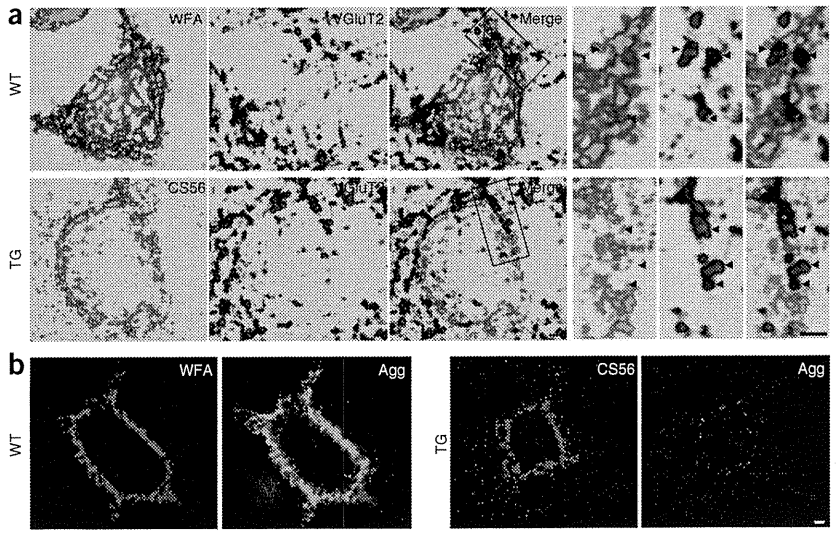

Figure 5 Chondroitin 6-sulfation–enriched PNNs show a diffuse structure and are unable to tightly surround thalamocortical synaptic contacts. (**a**) Three-dimensional reconstruction revealed a distinct meshwork of WFA$^+$ PNNs in controls. In contrast, CS56$^+$ PNNs in *C6ST-1* mice were sparse dot-like structures. Right, magnification of boxed regions in the left panels. VGluT2-labeled thalamocortical boutons (arrowheads) were embedded in the meshwork of WFA$^+$ PNNs in controls, whereas these boutons were not surrounded by CS56$^+$ PNNs in *C6ST-1* mice. (**b**) Staining with antibody to aggrecan (Agg) revealed a well-formed meshwork and almost the same pattern as that with WFA lectin in controls. In contrast, aggrecan staining of CS56$^+$ PNNs in *C6ST-1* mice appeared diffuse and less condensed over the soma. Scale bars represent 2 μm.

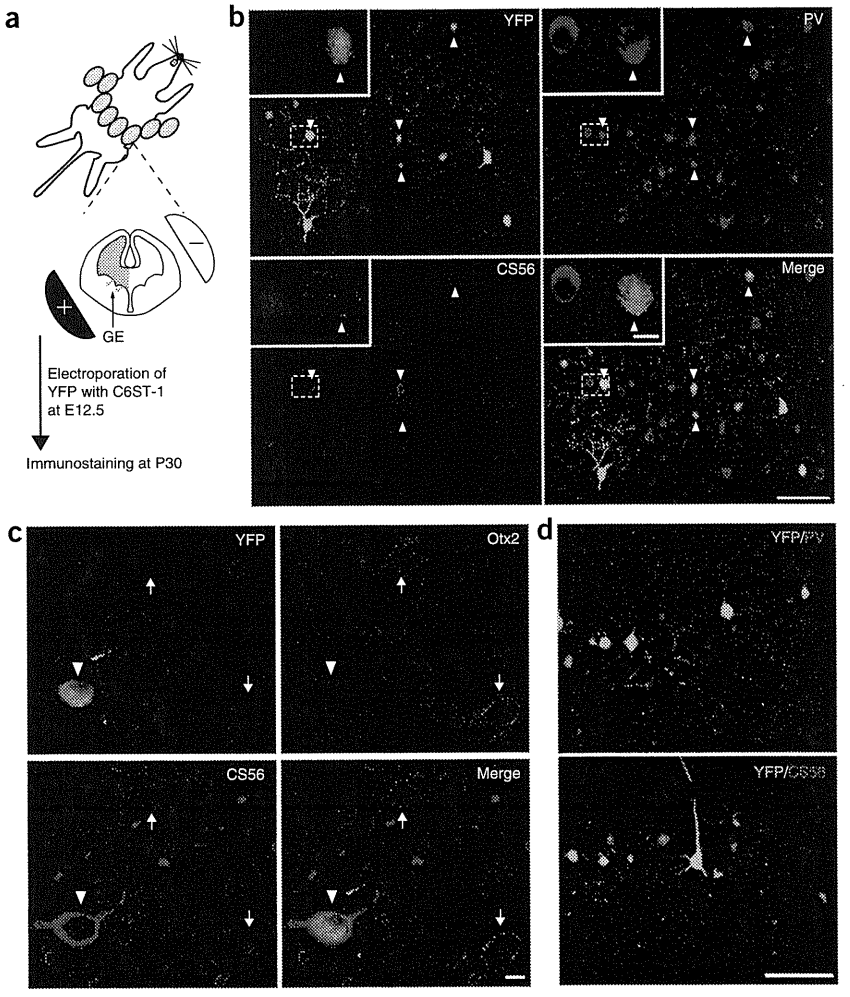

Figure 6 Overexpression of C6ST-1 in parvalbumin-expressing interneurons cell-autonomously affects PNN formation. (**a**) Experimental model for ganglionic eminence (GE)–directed electroporation. Wild-type interneurons were co-electroporated with *C6ST-1* and *YFP* at E12.5 and analyzed at P30. (**b**) CS56$^+$ PNNs were formed around co-transfected parvalbumin-expressing interneurons (arrowheads). Insets, magnification of boxed regions. Note that the transfected (right), but not the neighboring untransfected (left), parvalbumin-expressing interneurons were surrounded by CS56$^+$ PNNs. (**c**) Otx2 signal was not found in transfected parvalbumin-expressing interneurons surrounded by CS56$^+$ PNNs (arrowheads). Arrows indicate Otx2 accumulation in untransfected parvalbumin-expressing interneurons. (**d**) Overexpression of C6ST-1 in excitatory pyramidal neurons resulted in no YFP signal in parvalbumin-expressing interneurons and CS56$^+$ PNNs. Scale bars represent 100 μm (**b–d**) and 10 μm (insets in **b**).

feature of fast-spiking cells[29,30], was commonly found in both groups (**Fig. 7a**). No significant difference was found in the ratio of the last interspike interval to the second interspike interval (wild type, $n = 5$ neurons, 1.4 ± 0.15; *C6ST-1* transgenic, $n = 6$ neurons, 1.4 ± 0.18; $P > 0.7$). Furthermore, both groups showed another feature of fast-spiking cells: short-duration action potentials followed by fast afterhyperpolarizations[29,30] (**Fig. 7a**). Although no significant difference was found in the amplitude (wild type, $n = 5$ neurons, 16 ± 0.38 mV; *C6ST-1* transgenic, $n = 6$ neurons, 17 ± 0.49 mV; $P > 0.2$) or duration (wild type, $n = 5$ neurons, 26 ± 2.8 ms; *C6ST-1* transgenic, $n = 6$ neurons, 28 ± 2.9 ms; $P > 0.6$) of the afterhyperpolarization, the action potentials were significantly wider ($P < 0.009$) in *C6ST-1* transgenic mice than in wild-type mice (**Fig. 7b**). In addition, the resting membrane potential was significantly more depolarized ($P < 0.03$; **Fig. 7c**) in *C6ST-1* transgenic mice, although no difference was found in input resistance (wild type, $n = 5$ neurons, 145 ± 22.1 MΩ; *C6ST-1* transgenic, $n = 6$ neurons, 166 ± 20.7 MΩ; $P > 0.3$). Parvalbumin immunoreactivity was detected in all of the fast-spiking cells (four cells in wild-type mice and five cells in *C6ST-1* transgenic mice) in which we successfully conducted immunohistochemical examinations (**Fig. 7a**). A recent study on parvalbumin-expressing interneurons found that a shortening of spike width and a hyperpolarization of resting membrane potential proceeded in parallel with changes in the other membrane properties during postnatal development[31]. Thus, the overexpression of C6ST-1 prevented the maturation of some of the electrophysiological properties of parvalbumin-expressing interneurons.

In *C6ST-1* transgenic mice, parvalbumin-expressing interneurons may more easily initiate action potentials in response to excitatory inputs, as a result of their depolarized membrane potentials, and therefore inhibit their target cells more frequently than in wild-type mice. The shortening of spike width results in a reduction of transmitter release probability and short-term depression at the nerve terminals

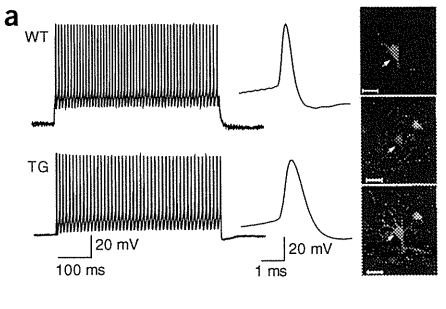

Figure 7 Overexpression of C6ST-1 prevents the maturation of the membrane properties of fast-spiking cells. (**a**) Example traces of spike discharges in response to a depolarizing current pulse (500-ms duration) in fast-spiking cells sampled from wild-type (current amplitude, 400 pA; top left) and *C6ST-1* mice (300 pA; bottom left). Middle, expanded traces show the second spike evoked by the current pulse. Calibrations were common to the two cells. Right, confocal images showing parvalbumin expression in a fast-spiking cell (arrows) sampled from a mouse. Staining for biocytin (top) and parvalbumin (middle) is shown together with a merged image (bottom). Scale bars represent 10 μm. (**b**) Half width of action potentials. (**c**) Resting membrane potential. *$P < 0.05$ (Student's t test) between *C6ST-1* and wild-type mice, and the numbers of fast-spiking cells were 5 (wild-type mice) and 6 (*C6ST-1* mice). Error bars represent s.e.m.

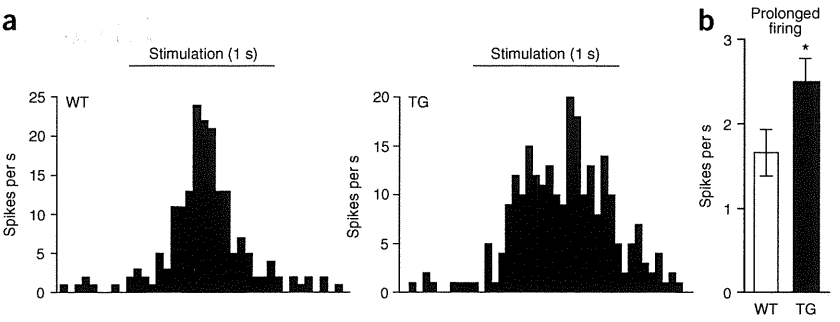

Figure 8 Comparison of visual responsiveness in visual cortical neurons between *C6ST-1* and wild-type mice. (**a**) Examples of post-stimulus time histograms for two cells, each of which was sampled from wild-type (left) and *C6ST-1* mice (right). Bars indicate the time (1 s) of presenting drifting gratings. (**b**) Mean firing rate during a 0.5-s period after the presentation of gratings. Values were calculated after subtraction of spontaneous firing rate. The number of cells was 40 (wild type) and 47 (*C6ST-1*). $*P < 0.05$ (Mann-Whitney test). Error bars represent s.e.m.

of parvalbumin-expressing interneurons[31]. Thus, individual action potentials in mature parvalbumin-expressing interneurons can inhibit their target cells effectively even when the firing frequency is high. In *C6ST-1* transgenic mice, short-term depression may remain stronger and the inhibitory effects of individual action potentials may therefore be weaker when parvalbumin-expressing interneurons fire frequently, as compared with wild-type mice. Thus, it is difficult to predict the overall influence of C6ST-1 overexpression on the inhibitory effects of parvalbumin-expressing interneurons.

To test whether the overexpression of C6ST-1 increased or decreased the inhibitory effects of parvalbumin-expressing interneurons, we examined prolonged firing by extracellular unit recordings from adult visual cortex. It is known that when the inhibitory effects of parvalbumin-expressing interneurons are reduced, visual cortical neurons showed prolonged firing after visual stimulus leave their receptive fields[5,32]. Visual responses were evoked repetitively by stimulation of the contralateral eye with sinusoidal gratings drifting for 1 s. On the whole, the visual responsiveness in *C6ST-1* transgenic mice was very similar to that in wild-type mice. No significant difference was found in orientation selectivity (wild type, $n = 40$ neurons, 0.51 ± 0.068 ; *C6ST-1* transgenic, $n = 47$ neurons, 0.50 ± 0.044; $P > 0.9$), mean firing rate during the optimal stimulation (wild type, $n = 40$ neurons, 7.8 ± 1.5 spikes per s; *C6ST-1* transgenic, $n = 47$ neurons, 6.5 ± 0.71 spikes per s; $P > 0.4$) or spontaneous firing rate (wild type, $n = 40$ neurons, 1.6 ± 0.18 spikes per s; *C6ST-1* transgenic, $n = 47$ neurons, 1.8 ± 0.18 spikes per s; $P > 0.3$) between the two groups. However, we noticed a tendency for prolonged firing after the end of the visual stimulus in *C6ST-1* transgenic mice (**Fig. 8a**), although the degree of prolonged firing seemed weaker than that found in mice deficient for a GABA-synthesizing enzyme[32]. We confirmed this tendency by comparing the mean firing rate during a 0.5-s period after the end of each drifting stimulus between *C6ST-1* transgenic and wild-type mice. The mean firing rate was significantly higher ($P < 0.003$) in *C6ST-1* transgenic than in wild-type mice (**Fig. 8b**). Thus, we conclude that overexpression of C6ST-1 maintains the inhibitory effects of parvalbumin-expressing interneurons in a slightly reduced state until adulthood, mainly as a result of a failure in spike shortening.

DISCUSSION

It has been proposed that there are two classes of molecular brakes that limit plasticity in adulthood[33]. Functional brakes regulate the balance between excitation and inhibition in local circuits. For example, Lynx1, a protein that inhibits nicotinic acetylcholine receptor signaling, restricts plasticity in adulthood through its influence on the balance between excitation and inhibition[34]. On the other hand, structural brakes, such as CSPGs and myelin-related proteins, are thought to limit plasticity by acting as physical barriers based on the mechanism by which they inhibit axonal growth[10,35]. However, our findings suggest an alternative model, in which specific sulfation patterns of chondroitin sulfate chains regulate the maturation of parvalbumin-expressing interneurons through the incorporation of Otx2. Because of the reduced accumulation of Otx2 in parvalbumin-expressing interneurons, *C6ST-1* transgenic mice had a reduced cortical inhibitory tone that did not reach the normal adult level; thus, these mice retained juvenile-like plasticity as adults. Originally, depletion of Otx2 was reported to prevent the initiation of the critical period[5]. Our data suggest that Otx2 also participates in the termination of the critical period. This is not surprising, as the maturation of cortical inhibitory interneurons is crucial for both the onset and termination of the critical period[2]. The onset and termination of the critical period can be accelerated by prematurely enhancing inhibitory transmission[2]. Conversely, reducing intracortical inhibition in adult animals reactivates ocular dominance plasticity after the critical period[36]. The cortical inhibition level has been proposed to cross two thresholds during development[37]. In this model, the critical period is initiated when the inhibition level reaches the first threshold. As development proceeds, the inhibition level increases further and terminates the critical period once it crosses the second threshold. Our data suggest that developmental changes in sulfation patterns of chondroitin sulfate may be required to cross the second threshold, but not the first.

Previous data showed that the number of parvalbumin-immunopositive cells and the intensity of parvalbumin staining were reduced by Otx2 knockdown[5]. We did not find such changes in *C6ST-1* transgenic mice, in spite of the impaired maturation of membrane properties of parvalbumin-expressing interneurons in these mice. Thus, expression levels of parvalbumin do not always correlate with the electrophysiological properties of parvalbumin-expressing interneurons. This idea is supported by the fact that parvalbumin deficiency dose not substantially affect PNN formation and the basic electrophysiological properties of parvalbumin-expressing interneurons[38]. Our results also suggest that the promotion of parvalbumin expression by Otx2 does not require the internalization of Otx2 into the neurons. Instead, a temporal interaction with some signaling molecules on the surface of neurons may be enough to promote parvalbumin expression. How Otx2 regulates parvalbumin-expressing interneuron function is currently unknown. We found that the reduced accumulation of Otx2 prevented the maturation of membrane properties of parvalbumin-expressing interneurons in *C6ST-1* transgenic mice; thus, Otx2 may be required for upregulation of K^+ channels of the K_v3 subfamily underlying brief action potentials[39] and other types of K^+ channels contributing to the hyperpolarization of resting membrane potentials of parvalbumin-expressing interneurons[31].

How the temporal shift of the 4S/6S ratio is regulated remains unknown. We investigated whether reducing cortical inhibition levels, which reactivate the critical period plasticity in adult mice[36],

also reduces the 4S/6S ratio by means of intracortical microperfusion of 3-mercaptopropionic acid (MPA), an inhibitor of GABA synthetic enzyme. However, the 4S/6S ratio in the visual cortex was not affected by MPA perfusion (**Supplementary Fig. 5**). The temporal shift of the 4S/6S ratio may be developmentally programmed and independent or upstream of visual experience or inhibition levels. Expression of several plasticity-associated genes, such as *cartilage link protein-1* (*Crtl1*) and *insulin-like growth factor-1*, is regulated by visual experience[40,41]. On the other hand, expression of myelin-related proteins is independent of visual experience[35]. PNNs formation partially depends on visual experience[10], suggesting that expression of some of these components is regulated by vision. Expression of Crtl1, which is required to stabilize PNNs formation, is downregulated by dark rearing, and *Crtl1*-deficient mice have attenuated PNN formation[40]. Thus, both experience-dependent (for example, Crtl1 expression) and experience-independent (for example, the 4S/6S ratio of chondroitin sulfate chains) factors seem to cooperate for PNN formation. Dysregulation of one of these factors may result in impaired PNN formation and persistent cortical plasticity.

The cellular origin of PNNs has been controversial. The glial origin of PNNs is supported by the fact that they are closely associated with glial processes and that some of their components are synthesized by glial cells[7–9]. In contrast, *in vitro* construction of PNNs in dissociated neuronal culture without glial cells suggests that they originate from neurons[42]. Our findings support the latter possibility, as it was possible to manipulate local PNN formation by parvalbumin-expressing interneuron autonomous elevation of chondroitin 6-sulfation. We also found that C6ST-1 overexpression in non–parvalbumin-expressing interneurons (that is, glial cells and pyramidal neurons) did not affect PNN formation around parvalbumin-expressing interneurons. This may be explained by the fact that the expression patterns of CSPG core protein vary among cell types. For example, brevican is produced in both neurons and glial cells[9], whereas aggrecan seems to be synthesized selectively by parvalbumin-expressing interneurons[43]. Our results indicate that sulfation patterns of CSPGs produced in parvalbumin-expressing interneurons largely contribute to PNN formation. According to a recent model of PNN formation, secreted CSPGs bind to both cell surface hyaluronan and tenascin-R to form massive macromolecules in the pericellular space[8]. Thus, the interaction between CSPGs with other PNN components may depend on the sulfation patterns of chondroitin sulfate. PNNs are very heterogeneous, probably because of differences in the glycan structure of CSPGs[23]. Our data may provide genetic evidence that the heterogeneity of PNNs results, at least in part, from differential sulfation patterns of chondroitin sulfate, which in turn differentially modulate parvalbumin-expressing interneuron function by regulating incorporation of Otx2.

PNN formation is not restricted to the visual cortex and can be found in many brain regions in which Otx2 is not found. Outside the visual cortex, PNNs may facilitate accumulation of other molecules that are secreted from presynaptic terminals. One such candidate is neuronal activity–regulated pentraxin, a secreted synaptic protein that binds to AMPA receptors at excitatory synapses on parvalbumin-expressing interneurons and regulates synaptic plasticity[44]. In the hippocampal neuronal culture, disruption of PNNs with chondroitinase ABC reduces accumulation of neuronal activity–regulated pentraxin on parvalbumin-expressing interneurons[44]. Dysfunction of parvalbumin-expressing interneurons has been implicated in not only cortical plasticity, but also some psychological disorders, such as schizophrenia[45]. It was recently reported that the number of PNNs was reduced in individuals with schizophrenia[46]. Thus, it will be fascinating to assess the contribution of sulfation patterns of chondroitin sulfate in models of these diseases.

METHODS

Methods and any associated references are available in the online version of the paper at http://www.nature.com/natureneuroscience/.

Note: Supplementary information is available on the Nature Neuroscience website.

ACKNOWLEDGMENTS

We thank T. Maruyama and F. Murakami for technical advises on the VEP recordings and *in utero* electroporation, respectively. This work was funded by a Grant-in-Aid for Scientific Research-B 21390025 (to H.K.), grants from the Scientific Research on Innovative Areas (23110003 and 23110004 to H.K. and Y.K.), and a Young Scientists grant (21890286 to S.M.) from Ministry of Education, Culture, Sports, Science & Technology, Japan.

AUTHOR CONTRIBUTIONS

S.M., Y.Y., Y.K. and H.K. designed and performed the research, analyzed the data and wrote the manuscript. S.M. and H.K. conceived the idea. C.T. produced *C6ST-1* transgenic mice.

COMPETING FINANCIAL INTERESTS

The authors declare no competing financial interests.

Published online at http://www.nature.com/natureneuroscience/.
Reprints and permissions information is available online at http://www.nature.com/reprints/index.html.

1. Wiesel, T.N. & Hubel, D.H. Single-cell responses in striate cortex of kittens deprived of vision in one eye. *J. Neurophysiol.* **26**, 1003–1017 (1963).
2. Hensch, T.K. Critical period plasticity in local cortical circuits. *Nat. Rev. Neurosci.* **6**, 877–888 (2005).
3. Gordon, J.A. & Stryker, M.P. Experience-dependent plasticity of binocular responses in the primary visual cortex of the mouse. *J. Neurosci.* **16**, 3274–3286 (1996).
4. Yazaki-Sugiyama, Y., Kang, S., Câteau, H., Fukai, T. & Hensch, T.K. Bidirectional plasticity in fast-spiking GABA circuits by visual experience. *Nature* **462**, 218–221 (2009).
5. Sugiyama, S. *et al.* Experience-dependent transfer of Otx2 homeoprotein into the visual cortex activates postnatal plasticity. *Cell* **134**, 508–520 (2008).
6. Sugahara, K. & Mikami, T. Chondroitin/dermatan sulfate in the central nervous system. *Curr. Opin. Struct. Biol.* **17**, 536–545 (2007).
7. Celio, M.R., Spreafico, R., De Biasi, S. & Vitellaro-Zuccarello, L. Perineuronal nets: past and present. *Trends Neurosci.* **21**, 510–515 (1998).
8. Galtrey, C.M. & Fawcett, J.W. The role of chondroitin sulfate proteoglycans in regeneration and plasticity in the central nervous system. *Brain Res. Rev.* **54**, 1–18 (2007).
9. Carulli, D. *et al.* Composition of perineuronal nets in the adult rat cerebellum and the cellular origin of their components. *J. Comp. Neurol.* **494**, 559–577 (2006).
10. Pizzorusso, T. *et al.* Reactivation of ocular dominance plasticity in the adult visual cortex. *Science* **298**, 1248–1251 (2002).
11. Bradbury, E.J. *et al.* Chondroitinase ABC promotes functional recovery after spinal cord injury. *Nature* **416**, 636–640 (2002).
12. Gama, C.I. *et al.* Sulfation patterns of glycosaminoglycans encode molecular recognition and activity. *Nat. Chem. Biol.* **2**, 467–473 (2006).
13. Mikami, T., Yasunaga, D. & Kitagawa, H. Contactin-1 is a functional receptor for neuroregulatory chondroitin sulfate-E. *J. Biol. Chem.* **284**, 4494–4499 (2009).
14. Nadanaka, S., Ishida, M., Ikegami, M. & Kitagawa, H. Chondroitin 4-*O*-sulfotransferase-1 modulates Wnt-3a signaling through control of E disaccharide expression of chondroitin sulfate. *J. Biol. Chem.* **283**, 27333–27343 (2008).
15. Kitagawa, H., Tsutsumi, K., Tone, Y. & Sugahara, K. Developmental regulation of the sulfation profile of chondroitin sulfate chains in the chicken embryo brain. *J. Biol. Chem.* **272**, 31377–31381 (1997).
16. Properzi, F. *et al.* Chondroitin 6-sulphate synthesis is up-regulated in injured CNS, induced by injury-related cytokines and enhanced in axon-growth inhibitory glia. *Eur. J. Neurosci.* **21**, 378–390 (2005).
17. Fox, K. & Wong, R.O. A comparison of experience-dependent plasticity in the visual and somatosensory systems. *Neuron* **48**, 465–477 (2005).
18. Maeda, N. *et al.* Heterogeneity of the chondroitin sulfate portion of phosphacan/6B4 proteoglycan regulates its binding affinity for pleiotrophin/heparin binding growth-associated molecule. *J. Biol. Chem.* **278**, 35805–35811 (2003).
19. Frenkel, M.Y. & Bear, M.F. How monocular deprivation shifts ocular dominance in visual cortex of young mice. *Neuron* **44**, 917–923 (2004).
20. Godement, P., Salaün, J. & Imbert, M. Prenatal and postnatal development of retinogeniculate and retinocollicular projections in the mouse. *J. Comp. Neurol.* **230**, 552–575 (1984).
21. Sato, M. & Stryker, M.P. Distinctive features of adult ocular dominance plasticity. *J. Neurosci.* **28**, 10278–10286 (2008).
22. Härtig, W., Brauer, K. & Brückner, G. Wisteria floribunda agglutinin-labeled nets surround parvalbumin-containing neurons. *Neuroreport* **3**, 869–872 (1992).

23. Matthews, R.T. *et al.* Aggrecan glycoforms contribute to the molecular heterogeneity of perineuronal nets. *J. Neurosci.* **22**, 7536–7547 (2002).
24. Erisir, A. & Dreusicke, M. Quantitative morphology and postsynaptic targets of thalamocortical axons in critical period and adult ferret visual cortex. *J. Comp. Neurol.* **485**, 11–31 (2005).
25. Marín, O. & Rubenstein, J.L. A long, remarkable journey: tangential migration in the telencephalon. *Nat. Rev. Neurosci.* **2**, 780–790 (2001).
26. Tanaka, D.H. *et al.* Random walk behavior of migrating cortical interneurons in the marginal zone: time-lapse analysis in flat-mount cortex. *J. Neurosci.* **29**, 1300–1311 (2009).
27. Borrell, V., Yoshimura, Y. & Callaway, E.M. Targeted gene delivery to telencephalic inhibitory neurons by directional *in utero* electroporation. *J. Neurosci. Methods* **143**, 151–158 (2005).
28. Kawaguchi, Y. & Kondo, S. Parvalbumin, somatostatin and cholecystokinin as chemical markers for specific GABAergic interneuron types in the rat frontal cortex. *J. Neurocytol.* **31**, 277–287 (2002).
29. Connors, B.W. & Gutnick, M.J. Intrinsic firing patterns of diverse neocortical neurons. *Trends Neurosci.* **13**, 99–104 (1990).
30. Kawaguchi, Y. Physiological subgroups of nonpyramidal cells with specific morphological characteristics in layer II/III of rat frontal cortex. *J. Neurosci.* **15**, 2638–2655 (1995).
31. Goldberg, E.M. *et al.* Rapid developmental maturation of neocortical FS cell intrinsic excitability. *Cereb. Cortex* **21**, 666–682 (2011).
32. Hensch, T.K. *et al.* Local GABA circuit control of experience-dependent plasticity in developing visual cortex. *Science* **282**, 1504–1508 (1998).
33. Bavelier, D., Levi, D.M., Li, R.W., Dan, Y. & Hensch, T.K. Removing brakes on adult brain plasticity: from molecular to behavioral interventions. *J. Neurosci.* **30**, 14964–14971 (2010).
34. Morishita, H., Miwa, J.M., Heintz, N. & Hensch, T.K. Lynx1, a cholinergic brake, limits plasticity in adult visual cortex. *Science* **330**, 1238–1240 (2010).
35. McGee, A.W., Yang, Y., Fischer, Q.S., Daw, N.W. & Strittmatter, S.M. Experience-driven plasticity of visual cortex limited by myelin and Nogo receptor. *Science* **309**, 2222–2226 (2005).
36. Harauzov, A. *et al.* Reducing intracortical inhibition in the adult visual cortex promotes ocular dominance plasticity. *J. Neurosci.* **30**, 361–371 (2010).
37. Jiang, B., Huang, Z.J., Morales, B. & Kirkwood, A. Maturation of GABAergic transmission and the timing of plasticity in visual cortex. *Brain Res. Brain Res. Rev.* **50**, 126–133 (2005).
38. Schwaller, B. *et al.* Parvalbumin deficiency affects network properties resulting in increased susceptibility to epileptic seizures. *Mol. Cell. Neurosci.* **25**, 650–663 (2004).
39. Rudy, B. & McBain, C.J. Kv3 channels: voltage-gated K^+ channels designed for high-frequency repetitive firing. *Trends Neurosci.* **24**, 517–526 (2001).
40. Carulli, D. *et al.* Animals lacking link protein have attenuated perineuronal nets and persistent plasticity. *Brain* **133**, 2331–2347 (2010).
41. Tropea, D. *et al.* Gene expression changes and molecular pathways mediating activity-dependent plasticity in visual cortex. *Nat. Neurosci.* **9**, 660–668 (2006).
42. Miyata, S., Nishimura, Y., Hayashi, N. & Oohira, A. Construction of perineuronal net–like structure by cortical neurons in culture. *Neuroscience* **136**, 95–104 (2005).
43. Lander, C., Zhang, H. & Hockfield, S. Neurons produce a neuronal cell surface–associated chondroitin sulfate proteoglycan. *J. Neurosci.* **18**, 174–183 (1998).
44. Chang, M.C. *et al.* Narp regulates homeostatic scaling of excitatory synapses on parvalbumin-expressing interneurons. *Nat. Neurosci.* **13**, 1090–1097 (2010).
45. Lewis, D.A., Hashimoto, T. & Volk, D.W. Cortical inhibitory neurons and schizophrenia. *Nat. Rev. Neurosci.* **6**, 312–324 (2005).
46. Pantazopoulos, H., Woo, T.U., Lim, M.P., Lange, N. & Berretta, S. Extracellular matrix-glial abnormalities in the amygdala and entorhinal cortex of subjects diagnosed with schizophrenia. *Arch. Gen. Psychiatry* **67**, 155–166 (2010).

ONLINE METHODS

Generation of *C6ST-1* transgenic mice. Full-length human *C6ST-1* cDNA was amplified by reverse transcription PCR (RT-PCR) using a human placenta cDNA library and cloned into the EcoRI site of a pCAG vector, which drives transgene expression using a chicken β-actin promoter and CMV enhancer[47] Plasmid DNA was injected into C57BL6 embryos, which were placed into pseudopregnant females to produce transgenic offspring. Transgenic mice were identified by Southern blot using tail DNA and were mated with C57BL6 wild-type mice. Mice were kept under specific pathogen–free conditions in an environmentally controlled clean room at the Institute of Laboratory Animals, Kobe Pharmaceutical University. All experiments were conducted according to institutional ethics guidelines for animal experiments and safety guidelines for gene manipulation experiments. All animal procedures were approved by the Kobe Pharmaceutical University Committee on Animal Research and Ethics.

Chondroitin sulfate disaccharide composition. Brains were removed and cortical regions were dissected according to a mouse brain atlas and homogenized in cold acetone. The air-dried powder was exhaustively digested with actinase E (Kaken Pharma) at 60 °C for 24 h. The digest was treated with 5% trichloroacetic acid (wt/vol) and the acid-soluble fraction was extracted with diethyl ether. The aqueous phase was neutralized and subjected to gel filtration on a PD-10 column (GE Healthcare). The flow-through fractions were collected, evaporated dry and dissolved in water. An aliquot of the sample was digested with chondroitinase ABC (Seikagaku) at 37 °C for 2 h. The digests were derivatized with a fluorophore, 2-aminobenzamide, and then analyzed by anion-exchange high-performance liquid chromatography (SLC-10A, Shimadzu) on a PA-03 column (YMC). Identification and quantification of the resulting disaccharides were achieved by comparison with chondroitin sulfate–derived authentic unsaturated disaccharides (Seikagaku), as described previously[48].

Monocular deprivation. Monocular deprivation began at P24–26 for critical period mice and P60–P90 in adult mice. The eyelid margins of the right eye were trimmed and sutured under intraperitoneal pentobarbital anesthesia and deprivation continued for 3 or 6 d until the recording. Mice were monitored daily to be sure that the sutured eye remained shut and uninfected. Animals whose eyelids did not fully seal shut were excluded from further experiments.

VEP recordings. Mice were anesthetized with intraperitoneal fentanyl and droperidol and then placed in a stereotaxic frame. A local anesthetic, lidocaine, was administered at pressure points caused by the stereotaxic frame. Body temperature was maintained at about 37 °C. A large portion of the skull overlying the visual cortex was carefully drilled and removed leaving the dura intact. Microelectrodes (300–500 kΩ, Frederick Haer & Co) were inserted into the binocular visual cortex (3 mm lateral of lambda) and advanced 450 μm into the cortex. At this depth, VEPs had their maximal amplitude. Stimuli consisted of full-field sine-wave gratings of 0% and 100% contrast (mean luminance 25 cd m^{-2}, area = 30 × 50 cm), reversing at 1 Hz, and were presented at 0.05 cycles per degree. These stimuli were generated by a VSG4/2 card (Cambridge Research System) and displayed on the face of a monitor (FlexScan T962, Eizo Nanao), which was placed in front of the animal (distance, 28.5 cm). VEPs were elicited by horizontal gratings. VEP amplitude was quantified by measuring the negative peak amplitude of average responses, as described previously[49].

Unit recordings. Adult mice (P60–90) were anesthetized with urethane (1.1 g per kg of body weight, intraperitoneal) supplemented by the sedative chlorprothixene (9 mg per kg of body weight, intramuscular). Unit recordings were conducted from the binocular zone of the primary visual cortex using a tungsten-in glass electrode (3–5 MΩ; Frederick Haer & Co). Cells were recorded across all layers. We analyzed spikes that originated from single neurons using an off-line spike-sorting procedure. Visual stimuli consisted of a full-field drifting sinusoidal grating at a temporal frequency of 2 Hz were applied to the eye contralateral to the recording hemisphere. These stimuli were generated in the Psychophysics Toolbox extensions of MATLAB (Mathworks) and displayed on the face of a monitor (Flexscan T962, Nanao, 160-Hz refresh rate), which was placed in front of the animal (distance, 28.5 cm). To characterize visual responsiveness, we varied the direction of gratings between 0–360° (12 steps) at the spatial frequency between 0.01 and 0.32 (six steps). The orientation selective index was calculated as the ratio of $(R_{pref} - R_{orth})/(R_{pref} + R_{orth})$ at the optimal spatial frequency in each cell, where R_{pref} was the response to the preferred direction and R_{orth} was the mean response of the two directions orthogonal to the preferred direction.

Whole-cell recordings from slice preparations. Coronal slices (300 μm) of primary visual cortex were prepared from mice at P30–34 under deep anesthesia with isoflurane. Slices were cut and recovered for 1 h in oxygenated (95% O_2 and 5% CO_2) artificial cerebrospinal fluid (ACSF) containing 126 mM NaCl, 3 mM KCl, 1.2 mM NaH_2PO_4, 1.3 mM $MgSO_4$, 2.4 mM $CaCl_2$, 26 mM $NaHCO_3$ and 10 mM glucose at 33 °C. Then slices were kept in the ACSF at 24–25 °C. During recording experiments, slices were perfused with ACSF at 24–25 °C. An infrared Olympus DIC microscope with a 40×, 0.8 NA water-immersion lens was used to visualize and target recording electrodes to nonpyramidal neurons located in and near layer 4. Patch pipettes (4–6 MΩ) were filled with an internal solution containing 130 mM potassium gluconate, 8 mM KCl, 1 mM $MgCl_2$, 0.6 mM EGTA, 10 mM HEPES, 3 mM Na^+-ATP, 0.5 mM Na^+-GTP, 10 mM sodium phosphocreatine and 0.3% biocytin (wt/vol) (pH 7.3 adjusted with KOH). Recordings were made using a Multiclamp 700B (Molecular Probes) in the current-clamp mode. For analysis, we selected cells with series resistance less than 20 MΩ and did not compensate the resistance. To assess the membrane properties of recorded cells, we stimulated cells with current pulses (duration, 500 ms) starting from −200 pA and increasing up to 700 pA in 100-pA steps. After recording, the recorded cells were visualized using Alexa Fluor 405–conjugated streptavidin (Molecular Probes).

Immunohistochemistry. Mice were perfused transcardially with phosphate-buffered saline (PBS) followed by 4% paraformaldehyde in PBS (wt/vol). Brains were removed and post-fixed overnight. Coronal sections (30 μm thick) were cut with a vibratome (Leica). Sections were permeabilized with 0.2% Triton X-100 (vol/vol) in PBS, blocked with 2% bovine serum albumin (wt/vol) in PBS, and incubated overnight at 25 °C with primary antibodies to parvalbumin (Swant, mouse monoclonal IgG, 1:5,000), CS56 (Seikagaku, mouse monoclonal IgM, 1:200), Otx2 (Santa Cruz Biotech, goat polyclonal IgG, 1:50 or Abcam, rabbit polyclonal IgG, 1:100), aggrecan (Millipore, rabbit polyclonal IgG, 1:400) or VGluT2 (Millipore, guinea pig polyclonal IgG, 1:500). TRITC-labeled WFA lectin (EY laboratories, 5 μg ml^{-1}) was used for staining perineuronal nets. Sections were incubated with the appropriate Alexa 488/568/647-labeled (Invitrogen) or Cy-5–labeled (Millipore) secondary antibodies for 1 h at 25 °C. After washing with PBS, sections were stained with Hoescht 33342 (2 μg ml^{-1}) to identify cell nuclei. Images were captured with an LSM 710 laser-scanning confocal microscope using a 10× objective (Carl Zeiss). For quantification of the number of WFA-, CS56-, parvalbumin- and Otx2-immunopositive cells, labeled cells were counted in a 1.0 × 1.2 mm area spanning all cortical layers of the primary visual cortex. For three-dimensional reconstruction, we randomly selected PNNs in layer 4 from both wild-type and *C6ST-1* transgenic mice. Images at 0.35-μm steps were acquired using a 63× objective and processed using ZEN software (Carl Zeiss).

***In utero* electroporation.** Ganglionic eminence–directed *in utero* electroporation was performed on E12.5 wild-type mice as described pereviously[32,33]. Briefly, 2–3 μl of a mixture of *pCAG-C6ST1* (1 μg μl^{-1}) and *pCAG-YFP* (1 μg μl^{-1}) plasmid solution was injected into the lateral ventricle using a pulled glass capillary. The head was clasped with a pair electrode (CUY650P2 or CUY650P5; NEPA Gene) at an angle of 30–60° from the horizontal plane. Square electric pulses (30 V for 50 ms, five times in 950-ms intervals) were passed using an electroporator (NEPA21, NEPA Gene).

Immunoblotting. Brains were homogenized in M-PER buffer (Thermo) containing protease inhibitor cocktail (Nacalai) and incubated on ice for 30 min. After centrifugation, protein concentrations of supernatants were determined by BCA assay kit (Thermo). Protein (200 μg) was digested with 5 milliunits of chondroitinase ABC for 2 h at 37 °C. Protein (10 μg) was separated by 5% acrylamide gel electrophoresis, transferred onto PVDF membrane (GE Healthcare), and incubated overnight at 4 °C with primary antibodies to aggrecan (Millipore, rabbit polyclonal IgG, 1:2,000), phosphacan (Developmental Studies Hybridoma Bank, mouse monoclonal IgG, 1:200) or brevican (BD Biosciences, mouse monoclonal IgG, 1:2,000). The blot was incubated with the appropriate horseradish peroxidase–labeled secondary antibodies for 1 h at 25 °C and developed with

the ECL detection system (GE Healthcare). The relative abundance of CSPG core proteins was quantified as the density of the band using ImageQuant TL software (GE Healthcare).

Labeling of retinogeniculate axons at dLGN. Mice under pentobarbital anesthesia received intravitreous injections of Alexa Fluor 488– and Alexa Fluor 594–conjugated cholera toxin B subunits (Invitrogen, 2.5 μl of 2 mg ml^{-1} in PBS) into the left and right eyes, respectively, with a 33 G needle. The needle was gently pulled out after being held in place for about 1 min. Mice were perfused at 24 h after injection. Brains were dissected, post-fixed and cut coronally into 100-μm-thick serial sections with a vibratome. Images of the dLGN at the largest cross-section were captured with a LSM 710 laser-scanning confocal microscope.

Quantitative real-time RT-PCR. Total RNA from the retina, dLGN and visual cortex was isolated with the RNeasy mini kit (Qiagen). cDNA was synthesized from 300 ng of total RNA using Moloney murine leukemia virus reverse transcriptase (Promega). We used primer sequences specific for *Otx2* (forward, 5′-CTCGACGTTCTGGAAGCTCT-3′; reverse, 5′-ACTGGCCACTTGTTCCACTC-3′) and *β-actin* (forward, 5′-AGAGGGA AATCGTGCGTGAC-3′; reverse, 5′-CAATAGTGATGCCTGGCCGT-3′). Quantitative real-time RT-PCR was performed using FastStart DNA Master plus SYBR Green I (Roche Applied Science) in a LightCycler ST300 (Roche Applied Science).

Primary cell culture. For primary astrocyte culture, dissociated cerebral cortical cells from P0 wild-type or *C6ST-1* transgenic mice were plated in 10-cm^2 dishes and grown in DMEM (Wako) containing 10% fetal bovine serum (vol/vol) and antibiotics until they reached confluence. Cells were split with trypsin and re-plated in 24-well dishes at a density of 100,000 cells per well (1.9 mm^2) on glass coverslips coated with poly-L-lysine (10 μg ml^{-1}). Medium was changed every 3 d until the cells reach confluence. At that time, the culture consisted mostly of astrocytes. Dissociated neuronal cultures were prepared from cerebral cortices of E18 wild-type or *C6ST-1* transgenic mice and plated onto the astrocyte monolayer at a density of 200,000 cells per well (1.9 mm^2). Cells were maintained up to 18 d in Neurobasal Medium (Gibco) supplemented with 2% B-27 (vol/vol) plus (Miltenyi Biotec), 2 mM glutamax I (Gibco) and antibiotics. Half of the culture medium was replaced every 3–4 d. The cultures were fixed with 4% paraformaldehyde and stained with various antibodies as described above.

Intracortical microperfusion of MPA. Osmotic minipumps (model 1007D, rate = 0.5 μl h^{-1}; Alzet) containing MPA (100 μM in saline) were connected to a cannula (gauge 30) and implanted stereotaxically into the left hemisphere (3 mm lateral to the midline, 2 mm anterior to lambda) of adult mice. MPA was continuously infused for 1 week into the left visual cortex. The left (MPA treated) and the right (control) visual cortex was dissected and homogenized in ice-cold acetone. Chondroitin sulfate disaccharide composition analysis was performed as described above.

Statistical analysis. Statistical significance was determined by using unpaired two-tailed Student's *t* test. Differences were considered to be significant with a *P* value less than 0.05.

47. Niwa, H., Yamamura, K. & Miyazaki, J. Efficient selection for high-expression transfectants with a novel eukaryotic vector. *Gene* **108**, 193–199 (1991).
48. Kitagawa, H., Kinoshita, A. & Sugahara, K. Microanalysis of glycosaminoglycan-derived disaccharides labeled with the fluorophore 2-aminoacridone by capillary electrophoresis and high-performance liquid chromatography. *Anal. Biochem.* **232**, 114–121 (1995).
49. Yoshimura, Y. *et al.* Involvement of T-type Ca^{2+} channels in the potentiation of synaptic and visual responses during the critical period in rat visual cortex. *Eur. J. Neurosci.* **28**, 730–743 (2008).